Viral manipulation of a novel mechanoresponsive signaling axis disassembles processing bodies

Elizabeth L. Castle[1], Pauline Douglas[3,5], Kristina D. Rinker[3,4,5], and Jennifer A. Corcoran[1,2,5]

[1]Department of Microbiology and Immunology, Dalhousie University, Halifax, NS, Canada
[2]Current address, Microbiology, Immunology and Infectious Diseases Department and Charbonneau Cancer Research Institute, University of Calgary, Calgary, AB, Canada.
[3]Department of Physiology and Pharmacology, University of Calgary, Calgary, AB, Canada.
[4]Department of Chemical and Petroleum Engineering and Centre for Bioengineering Research and Education, University of Calgary, Calgary, AB, Canada.
[5]Charbonneau Cancer Institute, University of Calgary, Calgary, AB, Canada.

Abstract

Processing bodies (PBs) are ribonucleoprotein granules important for cytokine mRNA decay that are targeted for disassembly by many viruses. Kaposi's sarcoma-associated herpesvirus is the etiological agent of the inflammatory endothelial cancer, Kaposi's sarcoma, and a PB-regulating virus. The virus encodes Kaposin B (KapB), which induces actin stress fibres (SFs) and cell spindling as well as PB disassembly. We now show that KapB-mediated PB disassembly requires actin rearrangements, RhoA effectors and the mechanoresponsive transcription activator, YAP. Moreover, ectopic expression of active YAP or exposure of ECs to mechanical forces caused PB disassembly in the absence of KapB. We propose that the viral protein KapB activates a novel mechanoresponsive signaling axis and links changes in cell shape and cytoskeletal structures to enhanced inflammatory molecule expression using PB disassembly. Our work implies that cytoskeletal changes in other pathologies will similarly impact the inflammatory environment.

Importance

For the first time, we demonstrate that processing bodies (PBs), cytoplasmic sites of RNA decay, are regulated by mechanical signaling events that alter actin dynamics. Using the overexpression of a viral protein called KapB, known previously to mediate PB disassembly, we show that actin stress fibers (SFs) and the mechanoresponsive transcription factor, YAP, are required for PB loss. We also show that other established mechanical signals (shear stress or stiff extracellular matrix) that lead to the formation of SFs and activate YAP also cause PB disassembly. This is important because it means that KapB activates, from the inside out, a pathway that links cell shape to post-transcriptional gene regulation via cytoplasmic PBs.

Introduction

Cells are exposed to a variety of environments and they respond to changes in external force by adjusting internal tension. These mechanical cues can be transmitted to the cell through changes to extracellular contact nodes (focal adhesions) and contractile actomyosin structures to maintain tension homeostasis (Friedland, Lee, and Boettiger 2009; Kong et al. 2009; del Rio et al. 2009; Grashoff et al. 2010; reviewed in Finch-Edmondson and Sudol 2016). Actin stress fibres (SFs) are cytoskeletal structures composed of thick actin bundles, often associated with focal adhesions (Vallenius 2013), that are force-responsive, maintaining cytoskeletal integrity in changing mechanical environments (Burridge and Guilluy 2016). SF formation is coordinated by the GTPase, RhoA; it activates the formin, mammalian diaphanous protein-1 (mDia1) to promote actin filament growth and Rho-associated coiled-coil kinase (ROCK) to promote actomyosin contractility through non-muscle myosin II (Watanabe et al. 1997; Amano et al. 1997; Kimura et al. 1996). These RhoA-effectors act together to promote the formation of contractile and stable actin filaments in response to mechanical and chemical stimuli (Watanabe et al. 1999).

External forces elicit a cascade of signals using actin as force transducers to alter gene expression. Activated serum response factor (SRF) transcription responds to actin polymerization (reviewed in Chai and Tarnawski 2002). SRF activation is negatively regulated by the cytoplasmic concentration of monomeric G-actin (Sotiropoulos et al. 1999). However, inducers of filamentous actin (e.g. active RhoA) deplete G-actin levels leading to SRF nuclear translocation and transcription (Sotiropoulos et al. 1999). A more recent example is the mechanoresponsive transcriptional coactivator Yes-associated protein (YAP), whose activity can be controlled by cell shape and cytoskeletal structure (Dupont et al. 2011; Wada et al. 2011; Halder, Dupont, and Piccolo 2012; Yu et al. 2012). YAP is nuclear and active in response to low cell-cell contact (Zhao et al. 2007), high stiffness of the extracellular matrix (ECM) (Dupont et al. 2011), in shear stress due to fluid flow (K.-C. Wang et al. 2016; Nakajima et al. 2017; Lai and Stainier 2017; H. J. Lee et al. 2017; Huang et al. 2016), or after G-protein coupled receptor (GPCR) activation (Yu et al. 2012). Most of these signals induce the activity of RhoA and promote the formation of SFs, (Noria et al. 2004; Lee and Kumar 2016), implicating actin cytoskeletal structures as requisite intermediates for YAP activation.

Nuclear YAP associates with its coactivators to mediate transcription of genes involved in cell proliferation, differentiation, survival and migration (Halder, Dupont, and Piccolo 2012).

Consistent with this, nuclear YAP is often pro-tumourigenic and drives progression of many oncogenic traits in a variety of cancers. These include the induction of cell stemness (Panciera et al. 2016), altered metabolism (C. Yang et al. 2018), cancer cell invasion/vascular remodeling (Calvo et al. 2013; Liu et al. 2018; Kimura et al. 2020), and altered growth and proliferation (Kapoor et al. 2014; Zanconato et al. 2015; Jang et al. 2017). Kaposi's sarcoma (KS) is an endothelial cell (EC) cancer that is strongly linked to Kaposi's sarcoma-associated herpesvirus (KSHV) (Chang et al. 1994; Russo et al. 1996; Zhong et al. 1996; Ganem 1997). KSHV establishes persistent, life-long infection of its human host, and displays two types of infection, latent and lytic. In KS, the majority of the tumour ECs are latently infected while lytic replication is rare; in part, because these cells die as a result of viral replication (Boshoff et al. 1995; Staskus et al. 1997; Umbach et al. 2010; Speck and Ganem 2010; Arias et al. 2014). That said, during their short lifetime lytic cells expel progeny virus and secrete large quantities of pro-inflammatory and angiogenic molecules, making even infrequent lytic replication an important driver of KS. A key contributor to this secretory phenotype is the constitutively active viral G protein-coupled receptor (vGPCR), a lytic viral protein (Montaner et al. 2006; Corcoran et al. 2012). Despite the paracrine contributors like vGPCR, the few gene products that are expressed during the KSHV latent cycle are central for viral tumourigenesis. Many features of *in vivo* KS are recapitulated by *in vitro* latent infection of primary ECs, or ectopic expression of individual KSHV latent genes, including enhanced proliferation and an elongated or 'spindled' morphology characteristic of KS. Spindling is induced by two KSHV latent genes, vFLIP (Grossmann et al. 2006) and Kaposin B (KapB; (Corcoran, Johnston, and McCormick 2015)). Spindled cells also secrete a variety of proinflammatory cytokines and angiogenic factors, to further promote tumour progression through inflammatory cytokine production (Ensoli 1998; Ciufo et al. 2001; Naranatt et al. 2003; Grossmann et al. 2006; Ojala and Schulz 2014). However, no information exists to demonstrate pro-tumourigenic YAP activation in KSHV latency, despite the fact that the vGPCR has been shown to activate YAP during KSHV lytic infection (Liu et al. 2015).

One way that KSHV latency promotes the pro-inflammatory and pro-tumourigenic KS microenvironment is via KapB-mediated disassembly of cytoplasmic ribonucleoprotein granules called processing bodies (PBs) (Corcoran, Johnston, and McCormick 2015). PBs are involved in many RNA regulatory processes such as RNA silencing, nonsense-mediated decay and mRNA decay (Eulalio, Behm-Ansmant, and Izaurralde 2007). We and others have shown that PBs are

the major site for the translational suppression or constitutive decay of human mRNAs that code for potent regulatory molecules such as proinflammatory cytokines (Franks and Lykke-Andersen 2007; Corcoran, Johnston, and McCormick 2015; Vindry et al. 2017; Blanco et al. 2014). There are ~4500 of these transcripts, all of which bear destabilizing AU-rich elements (AREs) in their 3'-untranslated regions (3'-UTRs) (Shaw and Kamen 1986; Shyu, Greenberg, and Belasco 1989; Chen and Shyu 1995; Winzen et al. 1999; Stoecklin, Mayo, and Anderson 2006; Franks and Lykke-Andersen 2007; Bakheet, Williams, and Khabar 2006; Bakheet, Hitti, and Khabar 2017). PB abundance and composition is extremely dynamic and responds to cellular stress (Sheth 2003; Kedersha and Anderson 2007; Aizer et al. 2008; Takahashi et al. 2011). Specifically, activation of the stress-responsive p38/MK2 MAP kinase pathway by KapB elicits PB disassembly and prevents constitutive ARE-mRNA turnover (Winzen et al. 1999; Docena et al. 2010; Corcoran et al. 2012; Corcoran and McCormick 2015; Corcoran, Johnston, and McCormick 2015). This is an important yet underappreciated regulatory mechanism that fine tunes the production of potent proinflammatory cytokines and angiogenic factors in KS.

Though PBs are dynamic and stress-responsive, the precise signaling events that lead to PB assembly or disassembly are not well understood. We showed previously that KapB binds and activates MK2, which then phosphorylates hsp27, complexes with p115RhoGEF, and activates RhoA to elicit PB disassembly (Corcoran, Johnston, and McCormick 2015; Garcia et al. 2009; McCormick and Ganem 2005). While it is well-established that RhoA coordinates SF formation (Ridley and Hall 1992; Watanabe et al. 1999; Schmitz et al. 2000; Hotulainen and Lappalainen 2006), the precise mechanism of how RhoA promotes PB disassembly is not appreciated (Corcoran, Johnston, and McCormick 2015; Takahashi et al. 2011). In an effort to better understand the regulation of PB disassembly by KapB and RhoA, we began by targeting downstream RhoA effectors reported to promote SF formation to determine if the proteins known to mediate cytoskeletal remodeling were also necessary for PB disassembly. We reasoned that at some point we would be able to uncouple the signaling events that led to SFs from those that led to PB disassembly. We were not. We now present data that conclusively shows KapB-mediated PB disassembly is dependent not only on RhoA, but on cytoskeletal structures, actomyosin contractility and the presence of the mechanoresponsive transcription transactivator, YAP. We also present the first evidence of elevated YAP levels in response to expression of a KSHV latent gene, KapB. We also extend these studies beyond their impact on viral

tumourigenesis, by determining the mechanical regulation of PB dynamics in the absence of KapB expression, and show that induced cell contractility, cytoskeletal structures and active YAP all precede PB disassembly. Using a viral protein from an oncogenic virus, we have discovered a novel mechanoresponsive signaling pathway that transduces signals from cell shape and cytoskeletal structures to YAP to control PBs, post-transcriptional regulators of cellular gene expression.

Results

RhoA effectors controlling SF formation are required for PB disassembly

We previously showed that KapB-mediated PB disassembly required RhoA (Corcoran, Johnston, and McCormick 2015). In this work, we investigated whether downstream RhoA effectors known to control SF formation also control PB disassembly. Mammalian diaphanous protein 1 (mDia1) and Rho-associated coiled-coil kinase (ROCK) are considered the main coordinators of RhoA-mediated SF formation (Watanabe et al. 1999; Tojkander, Gateva, and Lappalainen 2012). mDia1 is a formin that promotes actin filament polymerization (Watanabe et al. 1999). To examine whether mDia1 was required for KapB-mediated PB disassembly, we designed short hairpin RNAs (shRNAs) to silence mDia1 mRNA. KapB- and vector- expressing human umbilical vein endothelial cells (HUVECs) were transduced with mDia1-targeting shRNAs and selected. Silencing efficacy was confirmed with immunoblotting (Fig 1A). PB analysis was performed using CellProfiler to quantify immunofluorescence images stained for the hallmark PB-resident protein, Hedls, as described in detail in the methods (J. H. Yu et al. 2005; Kedersha et al. 2008). Knockdown of mDia1 increased PBs in KapB-expressing cells (Fig 1B, D). mDia1-sh1 showed a greater increase in PBs in comparison to mDia1-sh2 (Fig 1B), likely because mDia1-sh1 reduced protein expression by 90% whereas mDia1-sh2 reduced it by 40-50% (Fig 1A). To ensure that the loss of mDia1 did not increase PBs globally but rather that mDia1 contributed specifically to KapB-mediated PB disassembly, we calculated the ratio of PBs per cell in KapB-expressing cells and normalized to PBs per cell in vector controls. This is important because this calculation shows whether KapB is still able to disassemble PBs, relative to vector, in the context of mDia silencing. If the ratio is ≥1 after sh-mDia treatment, it indicates that KapB is no longer able to disassemble PBs in comparison to the vector control, and that mDia contributes directly to KapB-mediated PB disassembly. Conversely, if the ratio is ~ 0.4 to

0.6, it indicates that KapB can still disassemble PBs even in the context of sh-mDia treatment. In this case, we determined that silencing using both mDia1-sh1 and mDia1-sh2 restored the PB ratio in KapB:Vector cells to ~1, indicating that the ability of KapB to disassemble PBs is lost after mDia silencing and that this is a specific effect (Fig 1C). We note that this ratio will be reported in subsequent figures for every RNA silencing or drug treatment applied to test KapB-mediated PB disassembly. We also observed that mDia1 silencing did not eliminate SF formation (Fig 1D) but, instead, increased elongated cells with visible actin SFs across the cell in both vector and KapB conditions. The visible actin structures may represent different SF subtypes or actin bundles that compensate for the loss of mDia1 (Hotulainen and Lappalainen 2006).

ROCK promotes SF formation by increasing actin contractility and inhibiting actin severing activity (Julian and Olson 2014). Chemical inhibition of both isoforms of ROCK, ROCK1 and ROCK2, with Y-27632 (Ishizaki et al. 2000) restored PBs in KapB-expressing cells and increased the ratio of KapB:Vector PBs (Fig 2A-C). To determine whether PB disassembly is dependent on a single ROCK isoform, both ROCK1 and ROCK2 were knocked down with isoform-specific shRNAs. Knockdown efficacy was confirmed with immunoblotting (Fig S1). Independent knockdown of ROCK1 and 2 increased PBs counts in KapB-expressing cells (Fig 2D, F) and restored the ratio of KapB:Vector PBs counts (Fig 2E). This indicated that both ROCK1 and ROCK2 can contribute to KapB-mediated PB disassembly. ROCK2 knockdown showed more robust PB restoration, both in terms of PB counts and PB size, than that seen with ROCK1 knockdown (Fig 2D, F). Quantification of PB counts in control cells for both pan-ROCK inhibition and ROCK knockdown experiments is reported in Figure S1. While pan-ROCK inhibition and ROCK1 knockdown treatments both eliminate SFs, ROCK2 knockdown retains pronounced actin fibres in the cells (Fig 2F). Similar to mDia1 knockdown, this may indicate a compensatory mechanism to retain cell shape and suggests that only a subset of SFs may be required for PB disassembly. Taken together, these data show that inhibition of RhoA effectors that mediate SF formation can reverse KapB-mediated PB disassembly. Put another way, we have been unable to uncouple KapB-mediated SF formation from KapB-mediated PB disassembly.

ROCK phosphorylates and activates LimK, which then phosphorylates and inactivates cofilin, an actin-severing protein (Ohashi et al. 2000). In this way, ROCK promote SF formation.

To investigate the role of cofilin in KapB-mediated PB disassembly, shRNAs to knockdown cofilin expression were used (Fig S2A). Since ROCK activation results in less cofilin activity and reduced actin severing, we hypothesized that knockdown of cofilin in KapB-expressing cells would augment KapB-mediated PB disassembly. Knockdown of cofilin resulted in elongated cells with more SFs (Fig S2D). Cofilin knockdown also augmented PBs disassembly in KapB-expressing cells (Fig S2B, C). This indicates that inhibition of cofilin elicits PB disassembly and supports the hypothesis that by reducing cofilin activity to promote KapB-mediated SF formation, PB disassembly is enhanced.

G-actin concentration does not influence PB disassembly

Since we could not uncouple the signalling controlling SF formation from PB disassembly, we investigated whether changes in the concentration of monomeric G-actin, known to control cellular stress and SRF transcriptional responses (Sotiropoulos et al. 1999; Chambers et al. 2015), could be controlling PBs. Several studies have shown that increasing the proportion of filamentous actin decreases the cytoplasmic concentration of monomeric G-actin (Rasmussen et al. 2010; Bunnell et al. 2011; Chambers et al. 2015). We investigated if our phenotype, PB disassembly, was controlled by changes in the proportion of monomeric G-actin. To determine this, cells were treated with drugs known to either decrease or increase the proportion of monomeric G-actin. Jasplakinolide (Jasp) treatment decreases the G-actin fraction by facilitating actin nucleation and aberrant polymerization of actin (Bubb et al. 1999). Conversely, the actin polymerization inhibitor Cytochalasin D (CytD) caps the barbed end of actin filaments, preventing further elongation of the actin filament and increasing the free G-actin concentration (Wakatsuki et al. 2001). If the level of G-actin is the signal, we hypothesized that jasplakinolide, which decreases G-actin levels, would mediate PB disassembly, while cytochalasin D would do the opposite, and promote PB assembly. However, both treatments increased the PB count per cell (Fig S3A-C); these data indicate that the concentration of G-actin does not influence PB disassembly, and this is not the mechanism by which actin SF formation or enhanced activity of RhoA alters PB dynamics. These data are congruent with our mDia1 and ROCK knockdown experiments that show retention of visible F-actin bundles despite PB restoration.

α −actinin-1 activity promotes PB disassembly

The actinins are primarily known for their role in bundling actin fibres, though in non-muscle cells, α -actinin-1 and 4 do not mediate actin bundling to the same extent (Pellegrin and Mellor 2007). α -actinin-4 can, at times, localize to dorsal SFs, but it primarily mediates focal adhesion turnover and can act as a transcriptional regulator of genes associated with cell proliferation and differentiation (Honda et al. 1998; Kovac 2010; Honda 2015). α -actinin-1 primarily mediates SF bundling and formation, as well as focal adhesion maturation (Honda et al. 1998; Kovac 2010). Using immunofluorescence, we observed that the localization of the two isoforms seen in HUVECs (Fig S4A, B) was consistent with the reported localization and function, as α -actinin-1 was localized to actin fibres and α -actinin-4 was more diffusely cytoplasmic and nuclear, with some actin fibre localization (Honda et al. 1998; Kovac 2010). Since α -actinin-1 associated with SFs in HUVECs and overexpression of alpha-actinin-GFP has been shown to localize and reinforce SFs (Edlund, Lotano, and Otey 2001; Jackson et al. 2008), we asked whether its overexpression would promote PB disassembly. This was indeed the case, suggesting that enhancing SF bundling and focal adhesion maturation positively regulates PB disassembly (Fig S4C, D).

Changes in cytoskeletal contractility control PB disassembly

One of the downstream activities of the kinase, ROCK, is to phosphorylate myosin light chain to induce non-muscle myosin II (NMII)-mediated actomyosin contraction (Mutsuki Amano et al. 1996). Since ROCK is required for KapB-mediated PB disassembly, we determined whether functional actomyosin contractility is also required. KapB-expressing cells were treated with blebbistatin, which inhibits NMII-mediated actomyosin contractility by maintaining NMII in a conformation that is unable to bind actin filaments (Kovacs et al. 2004). Treatment of KapB-expressing cells with blebbistatin restored both PBs levels in KapB-expressing cells, as well as the KapB:Vector ratio of PBs (Fig 3A-C), indicating that contractility is required for KapB-induced PB disassembly. To determine if contraction would elicit the same phenotype in the absence of KapB, cells were treated with Calyculin A (CalA), an inhibitor of myosin light chain phosphatase that promotes NMII phosphorylation and actomyosin contraction (Asano and Mabuchi 2001). Inducing contraction with CalA decreased

counts of PBs (Fig 3D, E), again consistent with the hypothesis that actomyosin contractility controls PB disassembly.

Actomyosin contractility impacts cytoskeletal tension in adherent cells with SFs (Katoh et al. 1998; Tan et al. 2003). Additionally, both Jasp and CytD interfere with cytoskeletal tension (Rotsch and Radmacher 2000), and both increased PB counts (Fig S3). Since the mechanoresponsive transcription activator, YAP, is activated by increases to cytoskeletal tension via actomyosin contractility (Dupont et al. 2011), we predicted the following: 1) KapB expression increases cytoskeletal tension, 2) KapB expression will activate YAP and 3) both cytoskeletal tension and YAP will be required for PB disassembly. Though unable to directly test the first prediction, we now consider the role of YAP in KapB-mediated PB disassembly.

YAP activation induces PB disassembly

We investigated the cellular localization of YAP in KapB-expressing cells. KapB-transduced human umbilical vein endothelial cells (HUVECs) showed increased levels of nuclear YAP, as well as increased total YAP intensity by immunofluorescence, though the ratio of nuclear:cytoplasmic YAP was not markedly increased (Fig 4A). When YAP is phosphorylated by LATS, it is sequestered in the cytoplasm and transcriptionally inactive (Zhao et al. 2007). While YAP has multiple phosphorylation sites, phosphorylation at serine 127 is the most potent LATS-mediated phosphorylation site that promotes cytoplasmic distribution of YAP (Zhao et al. 2007). To investigate the phosphorylation status of YAP in KapB-expressing cells, levels of P(S127)-YAP and total YAP were measured by immunoblot. In KapB-expressing cells, there was a decrease in the ratio of P(S127)-YAP to total YAP suggesting that YAP is active when KapB is expressed (Fig 4B). We also observed an increase in total steady-state levels of YAP by immunoblotting, corroborating the increase in total YAP intensity seen by microscopy (Fig 4A, B). Taken together, these observations are the first evidence of enhanced YAP activity in response to expression of a KSHV latent gene. We next asked if active YAP in KapB-expressing cells can interact with TEAD and other transcription factors to elicit changes in gene expression (Vassilev et al. 2001). We used a TEAD-element luciferase assay to assess if canonical YAP transcription was activated. As a positive control, we used YAP 5SA, a mutant version of YAP that is unable to be phosphorylated and inactivated by the inhibitory kinase LATS (Zhao et al. 2007) and is thus considered constitutively active. YAP 5SA robustly activated the TEAD

element-containing firefly luciferase reporter (Fig S5A). Despite our observations of increased nuclear and total YAP, KapB did not induce the transcription of the TEAD element-containing firefly luciferase reporter (TEAD-Fluc; Fig S5A). Further, KapB did not increase steady-state mRNA levels of common YAP target genes CTGF, CYR61 and ANKRD1 by RT-qPCR, although these genes were elevated by YAP 5SA (Fig S5B). These data indicate despite the observation that YAP appears more abundant and nuclear in KapB-expressing cells, it is not activating transcription of its canonical gene targets.

We expressed shRNAs targeting YAP in KapB-expressing HUVECs to assess whether the altered levels of YAP impacted PB disassembly. Immunoblotting confirmed knockdown efficiency (Fig 4C). Knockdown of YAP increased PBs in KapB-expressing cells (Fig 4D-F). In the context of YAP knockdown, the KapB:Vector ratio of PBs counts was restored, indicating that YAP is required for KapB-mediated PB disassembly (Fig 4E) and suggesting that KapB is activating a mechanoresponsive signalling axis to elicit PB disassembly via YAP. We wondered if YAP was central to PB disassembly in the absence of KapB expression. To this end, we examined PBs after YAP 5SA expression. These cells displayed decreased number of PBs per cell, indicating that YAP 5SA elicited disassembly of PBs (Fig 5A, B). KapB-mediated PB disassembly correlates with increases in stability and levels of ARE-mRNA (Corcoran, Johnston, and McCormick 2015; McCormick and Ganem 2005). To examine whether YAP 5SA-mediated PB disassembly elicits the same changes in ARE-mRNAs, we used a luciferase assay previously established to measure the stability of ARE-mRNAs by measuring luminescence of an ARE-containing firefly luciferase reporter (Corcoran, Khaperskyy, and McCormick 2011). In this assay, as previously shown in Corcoran, Johnston, and McCormick (2015), KapB increased level of firefly luminescence indicating enhanced stability of its RNA transcript (Fig 5C). However, despite also inducing pronounced PB disassembly, YAP 5SA does not increase Fluc luminescence significantly more than the control construct (Fig 5C). This points to a divergence of KapB and active YAP outcome. Although PB disassembly is induced by the expression of both constitutively active YAP and KapB, active YAP increases the transcriptional activation of genes CTGF, CYR61 and ANKRD1 while KapB does not; conversely, KapB enhances the stability of ARE-mRNAs while active YAP does not.

YAP activators disassemble PBs

Since overexpression of constitutively active YAP leads to disassembly of PBs, we wanted to determine whether activation of endogenous YAP could do the same in the absence of KapB. We tested various upstream mechanical signals described to activate YAP for their ability to elicit PB disassembly: shear stress, low cell confluence and high ECM stiffness (Nakajima et al. 2017; Lee et al. 2017; Noria et al. 2004; Zhao et al. 2007; Dupont et al. 2011). For the first, we subjected HUVECs to shear stress by fluid flow (shear forces of 2 and 10 dyn/cm^2) and PBs were examined via immunofluorescence. Both treatments showed prominent cell elongation and resulted in robust PB disassembly (Fig 6A, B). To test if cell confluence regulates PB levels, HUVECs were seeded at low, medium and high densities. Cells at low confluence are reported to have active YAP and we predicted PBs would disassembly; however, the low-density monolayer displayed more PBs per cell then those at medium and high densities (Fig 6C, D). To test the impact of collagen stiffness on PB disassembly, HUVECs were plated on coverslips coated with increasing densities of collagen (0 to 64 μg/ cm^2). While collagen density does not perfectly reproduce matrix stiffness as it does not eliminate effects from increasing collagen-binding sites, increasing collagen densities correlate with increases in matrix stiffness (Yang, Leone, and Kaufman 2009; Lee et al. 2014; Joshi, Mahajan, and Kothapalli 2018). As collagen density increased, PBs decreased (Fig 6E, F). Taken together, these data indicate that PB disassembly occurred in response to mechanical stimuli known to require RhoA and altered cytoskeletal structures to activate YAP (shear stress and increased ECM concentration) (Zhao et al. 2012; Huang et al. 2016; Lee and Kumar 2016; Moreno-Vicente et al. 2018). Again, our model points to the importance of actin SF formation as a requisite precursor to PB disassembly irrespective of YAP activation status.

Shear stress mediated PB disassembly requires YAP

YAP responds to external forces that induce active RhoA, actin SFs, and pronounced cell elongation; in short, the typical behaviour of ECs in response to fluid flow. However, how YAP responds to shear stress is controversial (Wang et al. 2016; Huang et al. 2016; Lee et al. 2017; Nakajima and Mochizuki 2017). To verify YAP activation by continuous, unidirectional fluid flow in our system, HUVECs subjected to 2 and 10 dyn/cm^2 of shear stress were lysed and used for immunoblotting for P(S127)-YAP and total YAP. Shear stress the ratio of phosphor-YAP/YAP in both conditions, suggesting a higher proportion of active YAP (Fig 7A). To assess

335 if YAP was required for PB disassembly in response to shear stress, HUVECs transduced with
336 YAP-targeting shRNA were subjected to 10 dyn/cm^2 shear stress. PBs disassembled in cells
337 treated with a non-targeting shRNA when subjected to shear stress (Fig 7B, C), consistent with
338 earlier experiments (Fig 6A, B). When YAP was reduced by shRNA expression, ECs exposed to
339 shear stress had more PBs than control cells without shear (Fig 7B, C). Therefore, YAP is
340 required to disassemble PBs in response to shear stress. Taken together with our analysis of
341 KapB-mediated PB disassembly, these data suggest that when KapB is expressed, it turns on the
342 same mechanoresponsive signals that endothelial cells use to withstand mechanical forces like
343 shear, in the absence of an external stimulus. The outcome of both scenarios is YAP-dependent
344 disassembly of cytoplasmic PBs.
345
346 **Discussion**
347 In this manuscript, we have used a viral protein from an oncogenic virus to uncover the
348 relationship between cytoplasmic PBs and the mechanical regulation of actin SF formation. We
349 present data to support the existence of a novel mechanoresponsive pathway that links actin SFs,
350 actomyosin contractility, and the transcription transactivator YAP to the disassembly of PBs and
351 show that this pathway is hijacked by KapB during KSHV latency. Our major findings are as
352 follows. i) KapB-mediated PB disassembly requires actin SF effectors ROCK1/2 /mDia1 and is
353 enhanced by loss of the actin-severing protein, cofilin. ii) KapB-mediated PB disassembly is
354 reversed when blebbistatin is used to inhibit actomyosin contractility or after knockdown of the
355 mechanoresponsive transcription transactivator, YAP. iii) In the absence of KapB, we can induce
356 PB disassembly when we promote the formation of actin SFs, actomyosin contractility, and YAP
357 activity using overexpression of α−actinin-1 (promotes actin bundling into SFs and increases
358 cytoskeletal tension (Jackson et al. 2008)), Calyculin A (inhibits myosin light chain phosphatase
359 to promote actomyosin contraction (Asano and Mabuchi 2001)), or overexpression of active
360 YAP (YAP 5SA). Exposure of endothelial cells to the external forces created by shear stress or a
361 stiff extracellular matrix also induces PB disassembly in the absence of KapB. Together, these
362 data show for the first time, that PBs disassemble in response to mechanical signals that
363 transduce external forces from outside the cell to the actin cytoskeleton and that this is a pathway
364 used by endothelial cells to regulate gene expression in response to diverse stimuli. Moreover,
365 this work also highlights the remarkable pizzazz used by viruses to hijack cellular pathways. In

this case, we reveal that the viral protein KapB taps into this mechanoresponsive pathway to trigger mechanical changes to cytoskeletal structures and downstream effectors that would normally respond to force, thereby inducing PB disassembly from within the cell, rather than from without.

During the process of actin polymerization, the monomeric form of actin, globular actin (G-actin), aggregates in groups of three subunits or more to nucleate an actin filament, which extends into filaments via addition of further G-actin monomers through ATP-dependent polymerization (reviewed in Pollard 2016). 10 to 30 actin filaments (F-actin) bundle together into SFs, primarily using the α-actinin family for crosslinking (Small et al. 1998; Cramer, Siebert, and Mitchison 1997; Lazarides and Burridge 1975; Pellegrin and Mellor 2007). SFs with periodic distribution of actin-crosslinking proteins and non-muscle myosin II (NMII) are contractile structures (Katoh et al. 1998; Tan et al. 2003), but not all actin SFs function equally in this regard. For any structure to be able to generate tension, it must be tethered at the ends. Of the types of SFs (ventral SFs, dorsal SFs and transverse arcs; (Small et al. 1998)), ventral SFs are attached at both termini to the extracellular matrix (ECM) through focal adhesions and contain NMII, which imparts a contractile phenotype (Hotulainen and Lappalainen 2006; Small et al. 1998; Vallenius 2013). Dorsal SFs are attached through focal adhesions but do not contain NMII, and thus are not contractile (Small et al. 1998; Vallenius 2013). However, dorsal SFs are thought to work in concert with transverse arcs, which contain NMII but are not attached to focal adhesions, to mediate cellular contractility.

In this work, while we did not directly determine the subtype of actin SF structures that form in response to KapB-mediated RhoA activation, several features of our data suggest that the structures that are important for PB disassembly must be contractile and cytoskeletal tension. When both mDia1 and ROCK2 were silenced in KapB-expressing cells (Fig 1, 2), visible actin bundles are still apparent despite PB restoration in both contexts. This suggests that not all SF subtypes are required for our phenotype. In addition, blebbistatin treatment of KapB-expressing cells dramatically restored PBs; these data suggest that PB disassembly requires actin-mediated contractility rather than merely structural support (Fig 3). Furthermore, overexpression of α-actinin and shear stress increase cell stiffness (Lee et al. 2006; Jackson et al. 2008). Both treatments induced PB disassembly (Fig S4, 6), reinforcing the correlation between increasing cell tension and PB disassembly. Finally, our data show that YAP is required for PB disassembly

(Figs 4, 5, 7). YAP is mechanoresponsive; it becomes active when tension-forming actin structures are induced by external forces e.g. focal adhesion engagement by stiff ECM (Dupont et al. 2011; Sugimoto et al. 2018). As YAP activation and PB disassembly both rely on RhoA-induced cytoskeletal contractility, any activator of YAP that induces cytoskeletal tension through RhoA should mediate PB disassembly. Our data supports this notion, as shear stress forces and increasing collagen density both cause PB disassembly in the absence of KapB, while low confluence does not (Fig 6). We also know that GPCRs ($G_{11/12}$ and $G_q/11$) activate YAP in a RhoA-dependent manner (Yu et al. 2012) and LPA treatment or overexpression of KSHV-derived constitutively active vGPCR (both activate $G_{11/12}$) both induce PB disassembly (Corcoran et al. 2012; Corcoran and McCormick 2015), these findings support the conclusion that PB disassembly requires the formation of contractile actin structures like those associated with YAP transactivation responses.

KSHV is an oncogenic virus associated with the endothelial neoplasm, Kaposi's sarcoma (KS). Cells within the KS lesion display latent KSHV infection, proliferate abnormally, spindle, and release many pro-inflammatory and pro-tumourigenic mediators into the microenvironment. KapB expression alone recapitulates two of these key features, cell spindling and pro-inflammatory mediator production that results from enhanced stability of ARE-containing cytokine mRNAs that would normally shuttle to PBs for constitutive turnover (Corcoran, Johnston, and McCormick 2015). Our previous work showed that both phenotypes require KapB activation of the stress-responsive kinase, MK2, and the downstream activation of the GTPase RhoA (Corcoran, Johnston, and McCormick 2015; Corcoran and McCormick 2015). We also showed that the lytic vGPCR protein mediates PB disassembly and the concomitant stabilization of ARE-mRNAs; more recently ORF57 has been also reported to disrupt PBs (Corcoran et al. 2012; Sharma et al. 2019). The observation that KSHV encodes at least three separate gene products sufficient to drive PB disassembly suggests that PB disassembly is beneficial for some aspect of the infectious cycle. Further research is required to definitively address how PBs influence the KSHV infectious cycle and the fate of infected cells.

We and others observed that the presence or absence of PB punctae visible by microscopy directly correlates with the stability of ARE-mRNAs (Corcoran, Johnston, and McCormick 2015; Vindry et al. 2017; Blanco et al. 2014). We predicted that YAP- mediated PB disassembly would also promote ARE-mRNA stability. Indeed, several YAP-target genes

contain ARE elements in their 3'UTR, including CTGF and ANKRD1 (Shen and Stanger 2015; Bakheet, Hitti, and Khabar 2017). Shear forces also cause YAP-dependent PB disassembly and have previously been shown to upregulate many genes containing ARE-mRNAs (Vozzi et al. 2018; Bakheet, Hitti, and Khabar 2017). Comparison of the transcriptomic data from HUVECs subjected to shear stress from Vozzi et al (2018) (Accession: GEO, GSE45225) to entries in the ARE-mRNA database (Bakheet, Hitti, and Khabar 2017) showed a 20% enrichment in the proportion of genes that contained AREs in those transcripts that were upregulated by shear stress. This suggests that PB disassembly enables efficient translation of YAP targets by preventing recruitment of the ARE-containing transcripts to PBs. That said, overexpression of constitutively active YAP (YAP 5SA) disassembles PBs but does not increase stability of an ARE-containing firefly luciferase reporter (Fig 5) (Corcoran, Khaperskyy, and McCormick 2011)). This discrepancy may be due to different functional responses for different classes of AU-rich elements. Our ARE-containing luciferase reporter contains the AU-rich sequence derived from the 3'-UTR of GM-CSF, categorized in Cluster 5, whereas canonical YAP genes CTGF and ANKDR1 are in Clusters 1 and 2, respectively (Bakheet, Hitti, and Khabar 2017).

Data presented herein clearly implicate a requirement for YAP in the PB disassembly phenotype that is induced by KapB and by the external force, shear stress (Fig 4,7). However, the precise connection between YAP and PB disassembly is unclear. What we do know is that despite the clear reliance on YAP for PB disassembly, KapB does not increase expression of canonical YAP-regulated transcripts (Fig S5). Our data also show increases in total YAP, decreases in phosphorylated YAP; however, the ratio of nuclear:cytoplasmic YAP is not markedly altered (Fig 4). Taken together, these data suggest that PB disassembly is independent of YAP's role as a gene transactivator and may also be independent of YAP nuclear translocation. In the discussion that follows, we explore two possible models for how YAP may promote PB disassembly that are independent of its transactivation of canonical genes. *i) Cytoplasmic YAP promotes autophagic flux to promote PB catabolism*. Several studies link YAP with the regulation of the catabolic process of autophagy, though many of these are contradictory and suggest YAP-mediated autophagy control is cell type and context-dependent (Song et al. 2015; Liu et al. 2017; Pei et al. 2019; Totaro et al. 2019). Totaro et al. provided strong evidence to support that YAP promotes autophagic flux by promoting the expression of Armus, a Rab7-GAP that is required to mediate the fusion of autophagosomes with lysosomes in the final

degradative step of autophagy (Totaro et al. 2019). Their data also show that autophagic flux is a mechanoresponsive process; this supported by other studies wherein endothelium exposed to unidirectional shear stress upregulates autophagy (Liu et al. 2015; Yao et al. 2015; Wang et al. 2018; Das et al. 2018). These data are also consistent with preliminary data from our group that suggests that PB disassembly mediated by KapB requires autophagy (knockdown of Atg5 restores PBs [Robinson, Singh, Corcoran, unpublished data]) and the work of others (Hardy et al. 2017). In this model, we propose that the intermediate step(s) linking the requirement of YAP to the disappearance of PBs is the upregulation of autophagic flux, which results in the autophagic degradation of PB granules or PB components. *ii) YAP and PBs are antiviral* PBs are sites where innate immune factors congregate that are disrupted by most viruses during infection (Burdick et al. 2010; Li et al. 2012; Ostareck, Naarmann-de Vries, and Ostareck-Lederer 2014; Burgess and Mohr 2015; Cuevas et al. 2016; H. Wang et al. 2016; Lumb et al. 2017; Balinsky et al. 2017; Núñez et al. 2018; Ng et al. 2020). Indeed, KSHV encodes three separate proteins that all induce PB disassembly (Corcoran et al. 2012; Corcoran, Johnston, and McCormick 2015; Sharma et al. 2019). PBs are likely playing an as yet undefined and underappreciated role in regulating innate antiviral responses. YAP is also a novel and unappreciated negative regulator of innate immune signaling pathways. YAP blocks the ability of the innate immune kinase, TBK1, a downstream effector for several innate signaling pathways, to associate and activate its substrates (Zhang et al 2017). In so doing, YAP blocks downstream induction of interferons and increases viral replication (Zhang et al. 2017). This feature of YAP is independent of its ability to act as a transcriptional transactivator (Zhang et al. 2017). We speculate that KapB-induced PB disassembly, like active YAP, favours viral replication and survival and is promoted by KSHV in order to reshape subsequent antiviral innate immune responses.

In this manuscript, we describe the surprising convergence of two previously unrelated yet essential regulators of cellular gene expression – the mechanoresponsive transactivator YAP and cytoplasmic PBs, known regulators of AU-rich mRNA decay. We show that PB disassembly is mechanoresponsive; external forces that change cell shape and tension-forming cytoskeletal structures cause PB disassembly in a YAP-dependent manner. This discovery was made courtesy of the unique KSHV protein, KapB, and provides yet another example of how viruses have evolved surprising ways to manipulate their host and ensure their survival. In this case, KapB induces, from the inside out, a mechanoresponsive pathway to cause PB disassembly and

elevated YAP. Future study will untangle how these related mechanoresponsive events are induced by KSHV to better promote viral replication.

Materials and Methods

Antibodies, Plasmids and Reagents

The antibodies used in this study can be found in Table S1. The plasmids used in this study can be found in Table S2. Forward and reverse shRNA sequences were selected from the TRC Library Database in the Broad Institute RNAi consortium. YAP target shRNAs in pLKO.1 were obtained from Dr. C. McCormick (Dalhousie University, Halifax, Canada). Sequences for all shRNA oligonucleotides used for cloning are listed in Table S3. Cloning of shRNAs was conducted according to the pLKO.1 protocol (Addgene 2006). The chemical inhibitors used in this study can be found in Table S4.

Cell Culture

Human embryonic kidney 293T and 293A cells (HEK-293T/A, ATCC, Manassas, Virginia, US) and human cervical adenocarcinoma cells expressing a tetracycline-inducible repressor (HeLa Tet-Off, Clontech, Mountain View, California, US) were cultured in Dulbecco's Modified Eagle Medium (DMEM, Gibco, Carlsbad, California, US) supplemented with 10% heat-inactivated fetal bovine serum (Gibco), 100 U/mL penicillin, 100 μg/mL streptomycin, and 2 mM L-glutamine (Gibco). Pooled human umbilical vein endothelial cells (HUVECs, Lonza, Basel, Switzerland) were cultured in endothelial cell growth medium 2 (EGM-2, Lonza)). For HUVEC passaging, tissue culture plates were precoated for 30 min at 37˚C with 0.1% (w/v) porcine gelatin (Sigma, St. Louis, Missouri, US) in 1X PBS (Gibco).

Transfection for Lentivirus Production

HEK-293T cells at 70-80% confluence were transfected using 3.3 μg of the target lentiviral construct, 2 μg pSPAX2 and 1 μg pMD2.G with 1 mg/mL polyethyenimine (PEI, Sigma) in serum-free DMEM. After 5 to 6 h, media was replaced with antibiotic-free DMEM containing 10% FBS and 2 mM L-glutamine (Gibco). Transfected cells were incubated for 48 h at 37˚C to allow lentivirus production. The supernatant media containing viral particles was harvested and filtered through a 0.45 μm polyethersulfone (PES) filter (VWR, Randor, Pennsylvania, US) and aliquoted. Virus was stored at -80˚C until use.

Lentiviral Transduction

Lentivirus was supplied into wells of plated HUVECs in EGM-2 supplemented with 5 μg/mL hexadimethrine bromide (polybrene). After 24 h incubation, cells were selected with either 5 μg/mL blasticidin (Sigma) for 96 h, replacing the media and antibiotic at 48 h, or 1 μg/mL puromycin (Sigma) for 48 h. Following selection, HUVEC medium was replaced with EGM-2 without selection for at least 24 h recovery before further use.

Immunofluorescence

Immunofluorescence was performed as described previously (Corcoran, Johnston, and McCormick 2015). Briefly, cells were grown on coverslips (no. 1.5, Electron Microscopy Sciences, Hatfield, Pennsylvania, US). Following treatment, coverslips were fixed in 4% paraformaldehyde (PFA, Electron Microscopy Sciences) in PBS at 37°C for 10 min, permeabilized with 0.1% Triton-X100 (Sigma) in 1X PBS for 10 min at RT, and blocked in 1% Human AB serum (blocking buffer, Sigma) in 1X PBS for 1 h at RT. Coverslips were then incubated with diluted primary antibody in blocking buffer overnight at 4°C in a humidified chamber. After primary antibody incubation, coverslips were washed with 1X PBS and then incubated in fluorescently-tagged secondary antibody diluted in blocking buffer for 1 h at RT. If applicable, coverslips were stained with Phalloidin-conjugated Alexa-Fluor 647 (Invitrogen, 1:100) in 1X PBS for 1.5 h. Coverslips were mounted onto microscope slides (FisherBrand, Pittsburgh, Pennsylvania, US) using Prolong Gold Antifade Mounting Media (Invitrogen, Carlsbad, California, US). For coverslips that were used for Hedls puncta quantification, the following modifications to immunofluorescence were made: (1) Prior to permeabilization, coverslips were stained with wheat germ agglutinin (WGA) Alexa-647 conjugate (Invitrogen, 1:400) in 1X PBS for 10 min at RT. (2) Following secondary antibody incubation, coverslips were stained with 4',6-Diamidino-2-Phenylindole (DAPI, Invitrogen, 1:10,000) in 1X PBS for 5 min.

Confocal imaging was performed on the Zeiss LSM 880 Confocal Microscope (Charbonneau Microscopy Facility, University of Calgary, Calgary, Canada) at the 63X oil objective. CellProfiler imaging was performed on the Zeiss AxioImager Z2 (CORES facility, Dalhousie University, Halifax, Canada) or Zeiss AxioObserver (Charbonneau Microscopy Facility, University of Calgary) at the 40X oil objective.

Quantification of Processing Bodies Using CellProfiler Analysis

CellProfiler (cellprofiler.org) is an open source software for high-content image analysis (Kamentsky et al. 2011) and was used to develop an unbiased method for quantifying changes to PB dynamics. The pipeline used for quantifying PBs was structured as follows: To detect nuclei, the DAPI image was thresholded into a binary image. In the binary image, primary objects between 30 to 200 pixels in diameter were detected and defined as nuclei. Cells were identified as secondary objects in the WGA image using a propagation function from the identified nuclei, which determined the cell's outer edge. Using the parameters of a defined nucleus and cell border, the cytoplasm was then defined as a tertiary object. The Hedls channel image was enhanced using an "Enhance Speckles" function to identify distinct puncta and eliminate background staining. The cytoplasm image was then applied as a mask to the enhanced puncta image to ensure quantitation of only cytoplasmic puncta. Hedls puncta were measured in the cytoplasm of cells using a 'global thresholding with robust background adjustments' function as defined by the program. The threshold cut-off for identified Hedls puncta remained constant between all experiments with identical staining parameters. Puncta number per cell, intensity and locations with respect to the nucleus were measured and exported as .csv files and analyzed in RStudio. A template of the RStudio analysis pipeline is attached in Appendix A. Data was represented as fold change in Hedls puncta count per cell normalized to the vector puncta count. 'Relative Hedls Puncta/Cell (KapB/Vector)' demonstrates the KapB puncta count divided by vector puncta count, a ratio that was calculated within each treatment group for each biological replicate.

Protein Electrophoresis and Immunoblotting

Cells were lysed in 2X Laemmli buffer (20% glycerol, 4% SDS, 120 mM Tris-HCl), between 150 to 300 μL, depending on cell density. Lysates were homogenized with a 0.21-gauge needle, and supplemented to contain 0.02% (w/v) bromophenol blue (Sigma) and 0.05 M dithiothreitol (DTT, Sigma), then heated at 95˚C for 5 min. 7.5 or 12% TGX Stain-Free SDS-polyacrylamide gels (BioRad) were cast according to the instructions of the manufacturer and 5 to 15 μg of total protein were subjected to SDS gel electrophoresis using 1X SDS running buffer (25 mM Tris, 192 mM Glycine, 0.1% SDS). Precision Plus Protein All Blue Prestained Protein Standards (BioRad, Hercules, California, US) was used as a molecular weight marker. After electrophoresis, gels were UV-activated using the ChemiDocTouch (BioRad) Stain-Free Gel

setting with automated exposure for 45 s. The protein was transferred to low-fluorescence polyvinylidene difluoride (PVDF) membranes (BioRad) on the Trans-Blot Turbo Transfer System (BioRad) according to the instructions of the manufacturer. Following transfer, total protein amounts on membranes were imaged on the ChemiDocTouch using the Stain-Free Membrane setting with automated exposure. Membranes were then blocked using 5% BSA (Sigma) in 1X TBS-T (150 nM NaCl, 10 mM Tris, pH 7.8, 0.01% Tween-20) for 1 h at RT. Primary antibody was diluted in 2.5% BSA in 1X TBS-T. Membranes were incubated in primary antibody solution overnight at 4°C with rocking. The following day, membranes were washed 3 times for 5 min in 1X TBS-T. Membranes were incubated with the appropriate secondary antibody, conjugated to horseradish peroxidase (HRP) for 1 h at RT. Membranes were washed 4 times for 5 min in 1X TBS-T. Clarity™ Western ECL Blotting Substrate (BioRad) was mixed at a 1:1 ratio and applied to the membrane for 5 min. Chemiluminescent signal was imaged on ChemiDocTouch Chemiluminescence setting. Band intensity was quantified using ImageLab software (BioRad), normalizing to total protein.

Quantitative Reverse-Transcriptase Polymerase Chain Reaction (qRT-PCR)

Cells were lysed in 250 μL RLT buffer (Qiagen, Hilden, Germany) and RNA was extracted using the RNeasy Plus Mini kit (Qiagen) according to the manufacturer's instructions. Complementary DNA (cDNA) was synthesized from 1 μg of total RNA using the qScript cDNA SuperMix (QuantaBio, Hilden, Germany) according to the manufacturer's instructions. Real-time quantitative PCR with SsoFast EvaGreen qPCR MasterMix (BioRad) was used to quantify the fold-change in mRNA abundance. Relative fluorescence was quantified using CFX Connect (BioRad). All qRT-PCR primers efficiencies were between 90-110% in HUVECs and sequences are found in Table S5.

Luciferase Assay for TEAD Transcriptional Activity

HEK-293A cells were seeded in antibiotic-free DMEM at 75,000 cells/well. Mixtures of 500 ng of the target construct (pcDNA (Vector), pcDNA-KapB (KapB), p1XFLAG or p2XFLAG-YAP 5SA), 450 ng 8X-GTIIC luciferase reporter, 50 ng TREX-Renilla luciferase reporter and 3 μL FuGENE HD Transfection Reagent (Promega, Madison, Wisconsin, US) were transfected into HEK-293A cells. After 36 h, DMEM containing only 2 mM L-glutamine (starvation media) was supplied to the cells. Twelve hours after addition of starvation media, cells were lysed in 200 μL passive lysis buffer (Promega) and luciferase activity was assayed

using the Dual-Luciferase Reporter Assay System (Promega) according to the manufacturer's instructions. Luminescence was measured using the GloMax Luminometer (Promega).

Luciferase Assay for Stability of mRNA with AU-Rich Elements

This technique is described in Corcoran, Khaperskyy, and McCormick (2011). Briefly, Hela-Tet Off cells were seeded in antibiotic-free DMEM at 100,000 cells/well. Mixtures of 900 ng of the target construct (pcDNA (Vector), pcDNA-KapB (KapB), p1XFLAG or p2XFLAG-YAP 5SA), 90 ng TREX-Firefly ARE luciferase, 10 ng TREX-Renilla luciferase and 3 μL FuGENE HD Transfection Reagent (Promega) were transfected into Hela Tet-Off cells. After 36 h, 1 μg/mL doxycycline was supplied to the cells to inhibit further transcription of each reporter. Twelve hours after addition of doxycycline, cells were lysed in 200 μL passive lysis buffer (Promega) and luciferase activity was assayed using the Dual-Luciferase Reporter Assay System (Promega) according to the manufacturer's instructions. Luminescence was measured using the GloMax Luminometer (Promega).

Collagen-Coating for Altering Matrix Stiffness

Coverslips (no. 1.5, Electron Microscopy Sciences) were coated with a dilution series (0 to 64 μg/cm^2) of rat-tail collagen-1 (Gibco) in 0.02 M acetic acid for 4 h at RT. Slides were sterilized with UV irradiation and washed with 2 times with sterile 1X PBS prior to seeding cells.

Unidirectional Fluid Flow for Endothelial Cell Shear Stress

A parallel-plate flow chamber was used to expose ECs to shear stress. The system was described in detail in Gomez-Garcia et al. (2018). Briefly, cleaned, unfrosted microscope slides (Cole-Parmer, Vernon Hills, Illinois, US) were coated for 4 h at RT with rat-tail collagen-1 (Gibco) in 0.02 M acetic acid for a resultant 8.3 μg/cm^2 collagen density. Slides were sterilized with UV irradiation and washed 2 times with sterile 1X PBS. HUVECs were seeded at a density of 350,000 cells/slide and cultured for 24 h. Forty-five mL of EGM-2 supplemented with dextran (Spectrum Chemical, New Brunswick, New Jersey, US) for a resultant 3 cP viscosity was added to the stock media bottle. The stock media bottle was connected with the associated tubing and pulse dampener. Slides with seeded cells were inserted onto the flow chamber, a gasket (Specialty Manufacturing, Calgary, Canada) was added, and the system was sealed shut and attached to the flow loop following the outlet of a pulse dampener. The rate of fluid flow was started at 0.3 L/min and doubled every 15 min until final flow rates of 0.6 L/min and 2.7 L/min

644 were reached, corresponding to shear stress rates of 2 and 10 dyn/cm^2. Following 21 h, cells were
645 removed and immediately fixed for immunofluorescence or lysed for immunoblotting.
646 **Statistical Analysis**
647 Statistical analysis was performed in GraphPad Prism 8.0 software. Significance was
648 determined using a ratio paired t-test or repeated measures analysis of variance (ANOVA). One-
649 tailed ratio paired t-tests were applied in comparisons specifically examining PB restoration in
650 KapB-expressing cells as a directional hypothesis. In all other comparisons, two-tailed ratio
651 paired t-tests were applied. Significance was determined at $p = 0.05$. Each biological replicate
652 for CellProfiler quantification consisted of 6 images of each treatment in a given experiment,
653 counting approximately 100 to 200 cells per treatment.
654

655 **References**

656 Aizer, Adva, Yehuda Brody, Lian Wee Ler, Nahum Sonenberg, Robert H. Singer, and Yaron
657 Shav-Tal. 2008. "The Dynamics of Mammalian P Body Transport, Assembly, and
658 Disassembly In Vivo." *Molecular Biology of the Cell* 19 (11): 4154–66.
659 https://doi.org/10.1091/mbc.E08.
660 Amano, M, K Chihara, K Kimura, Y Fukata, N Nakamura, Y Matsuura, and K Kaibuchi. 1997.
661 "Formation of Actin Stress Fibers and Focal Adhesions Enhanced by Rho-Kinase." *Science*
662 275 (5304): 1308–11. https://doi.org/10.1126/science.275.5304.1308.
663 Amano, Mutsuki, Masaaki Ito, Kazushi Kimura, Yuko Fukata, Kazuyasu Chihara, Takeshi
664 Nakano, Yoshiharu Matsuura, and Kozo Kaibuchi. 1996. "Phosphorylation and Activation
665 of Myosin by Rho-Associated Kinase (Rho-Kinase)." *The Journal of Biological Chemistry*
666 271 (34): 20246–49. https://doi.org/10.1074/jbc.271.34.20246.
667 Arias, Carolina, Ben Weisburd, Noam Stern-Ginossar, Alexandre Mercier, Alexis S. Madrid,
668 Priya Bellare, Meghan Holdorf, Jonathan S. Weissman, and Don Ganem. 2014. "KSHV 2.0:
669 A Comprehensive Annotation of the Kaposi's Sarcoma-Associated Herpesvirus Genome
670 Using Next-Generation Sequencing Reveals Novel Genomic and Functional Features."
671 *PLoS Pathogens* 10 (1). https://doi.org/10.1371/journal.ppat.1003847.
672 Asano, Yukako, and Issei Mabuchi. 2001. "Calyculin-A, an Inhibitor for Protein Phosphatases,
673 Induces Cortical Contraction in Unfertilized Sea Urchin Eggs." *Cell Motility and the*
674 *Cytoskeleton* 48 (4): 245–61. https://doi.org/10.1002/cm.1013.
675 Bakheet, Tala, Edward Hitti, and Khalid S A Khabar. 2017. "ARED-Plus: An Updated and
676 Expanded Database of AU-Rich Element-Containing MRNAs and Pre-MRNAs." *Nucleic*
677 *Acids Research* 46 (October 2017): 2017–19. https://doi.org/10.1093/nar/gkx975.
678 Bakheet, Tala, Bryan R G Williams, and Khalid S a Khabar. 2006. "ARED 3.0: The Large and
679 Diverse AU-Rich Transcriptome." *Nucleic Acids Research* 34 (Database issue): D111–14.
680 https://doi.org/10.1093/nar/gkj052.
681 Balinsky, Corey A., Hana Schmeisser, Alexandra I. Wells, Sundar Ganesan, Tengchuan Jin,
682 Kavita Singh, and Kathryn C. Zoon. 2017. "IRAV (FLJ11286), an Interferon-Stimulated
683 Gene with Antiviral Activity against Dengue Virus, Interacts with MOV10." Edited by
684 Michael S. Diamond. *Journal of Virology* 91 (5). https://doi.org/10.1128/JVI.01606-16.
685 Blanco, Fernando F, Sandhya Sanduja, Natasha G Deane, Perry J Blackshear, and Dan a Dixon.

686 2014. “Transforming Growth Factor β Regulates P-Body Formation through Induction of
687 the MRNA Decay Factor Tristetraprolin.” *Molecular and Cellular Biology* 34 (2): 180–95.
688 https://doi.org/10.1128/MCB.01020-13.
689 Boshoff, Chris, Thomas F Schulz, Margaret M Kennedy, Andrew K Graham, Cyril Fisher, Alero
690 Thomas, J O’D. McGee, Robin a Weiss, and John J O’Leary. 1995. “Kaposi’s Sarcoma-
691 Associated Herpesvirus Infects Endothelial and Spindle Cells.” *Nature Medicine* 1 (12):
692 1274–78. https://doi.org/10.1038/nm1295-1274.
693 Bubb, Michael R, Ilan Spector, Bret B Beyer, and Katina M. Fosen. 2000. “Effects of
694 Jasplakinolide on the Kinetics of Actin Polymerization.” *Journal of Biological Chemistry*
695 275 (7): 5163–70. https://doi.org/10.1074/jbc.275.7.5163.
696 Bunnell, Tina M., Brandon J. Burbach, Yoji Shimizu, and James M. Ervasti. 2011. “β-Actin
697 Specifically Controls Cell Growth, Migration, and the G-Actin Pool.” Edited by Paul
698 Forscher. *Molecular Biology of the Cell* 22 (21): 4047–58. https://doi.org/10.1091/mbc.e11-
699 06-0582.
700 Burdick, Ryan, Jessica L. Smith, Chawaree Chaipan, Yeshitila Friew, Jianbo Chen, Narasimhan
701 J. Venkatachari, Krista A. Delviks-Frankenberry, Wei-Shau Hu, and Vinay K. Pathak.
702 2010. “P Body-Associated Protein Mov10 Inhibits HIV-1 Replication at Multiple Stages.”
703 *Journal of Virology* 84 (19): 10241–53. https://doi.org/10.1128/jvi.00585-10.
704 Burgess, Hannah M., and Ian Mohr. 2015. “Cellular 5′-3′ MRNA Exonuclease Xrn1 Controls
705 Double-Stranded RNA Accumulation and Anti-Viral Responses.” *Cell Host and Microbe*
706 17 (3): 332–44. https://doi.org/10.1016/j.chom.2015.02.003.
707 Burridge, Keith, and Christophe Guilluy. 2016. “Focal Adhesions, Stress Fibers and Mechanical
708 Tension.” *Experimental Cell Research* 343 (1): 14–20.
709 https://doi.org/10.1016/j.yexcr.2015.10.029.
710 Calvo, Fernando, Nil Ege, Araceli Grande-Garcia, Steven Hooper, Robert P. Jenkins, Shahid I.
711 Chaudhry, Kevin Harrington, et al. 2013. “Mechanotransduction and YAP-Dependent
712 Matrix Remodelling Is Required for the Generation and Maintenance of Cancer-Associated
713 Fibroblasts.” *Nature Cell Biology* 15 (6): 637–46. https://doi.org/10.1038/ncb2756.
714 Chai, J., and Andrzej S. Tarnawski. 2002. “Serum Response Factor: Discovery, Biochemistry,
715 Biological Roles and Implications for Tissue Injury Healing.” *Journal of Physiology and*
716 *Pharmacology* 53 (2): 147–57. https://doi.org/10.1007/s12630-011-9636-x.

717 Chambers, Joseph E, Lucy E Dalton, Hanna J Clarke, Elke Malzer, Caia S Dominicus, Vruti
718 Patel, Greg Moorhead, David Ron, and Stefan J Marciniak. 2015. "Actin Dynamics Tune
719 the Integrated Stress Response by Regulating Eukaryotic Initiation Factor 2α
720 Dephosphorylation." *ELife* 4 (March). https://doi.org/10.7554/eLife.04872.
721 Chang, Y, E Cesarman, M S Pessin, F Lee, J Culpepper, D M Knowles, and P S Moore. 1994.
722 "Identification of Herpes-like DNA Sequences in AIDS-Associated Kaposi's Sarcoma."
723 *Science* 266: 1865–69. https://doi.org/10.1126/science.7997879.
724 Chen, C Y, and a B Shyu. 1995. "AU-Rich Elements: Characterization and Importance in
725 MRNA Degradation." *Trends in Biochemical Sciences* 20 (11): 465–70.
726 https://doi.org/10.1016/S0968-0004(00)89102-1.
727 Ciufo, D M, J S Cannon, L J Poole, F Y Wu, P Murray, R F Ambinder, and G S Hayward. 2001.
728 "Spindle Cell Conversion by Kaposi's Sarcoma-Associated Herpesvirus: Formation of
729 Colonies and Plaques with Mixed Lytic and Latent Gene Expression in Infected Primary
730 Dermal Microvascular EndCiufo, D. M., Cannon, J. S., Poole, L. J., Wu, F. Y., Murray,
731 P.,." *Journal of Virology* 75 (12): 5614–26. https://doi.org/10.1128/JVI.75.12.5614-
732 5626.2001.
733 Corcoran, Jennifer A., Benjamin P. Johnston, and Craig McCormick. 2015. "Viral Activation of
734 MK2-Hsp27-P115RhoGEF-RhoA Signaling Axis Causes Cytoskeletal Rearrangements, P-
735 Body Disruption and ARE-MRNA Stabilization." Edited by Erle S. Robertson. *PLoS*
736 *Pathogens* 11 (1): e1004597. https://doi.org/10.1371/journal.ppat.1004597.
737 Corcoran, Jennifer A., Denys A. Khaperskyy, Benjamin P. Johnston, Christine A. King, David P.
738 Cyr, Alisha V. Olsthoorn, and Craig McCormick. 2012. "Kaposi's Sarcoma-Associated
739 Herpesvirus G-Protein-Coupled Receptor Prevents AU-Rich-Element-Mediated MRNA
740 Decay." *Journal of Virology* 86 (16): 8859–71. https://doi.org/10.1128/JVI.00597-12.
741 Corcoran, Jennifer A., Denys A. Khaperskyy, and Craig McCormick. 2011. "Assays for
742 Monitoring Viral Manipulation of Host ARE-MRNA Turnover." *Methods* 55 (2): 172–81.
743 https://doi.org/10.1016/j.ymeth.2011.08.005.
744 Corcoran, Jennifer A, and Craig McCormick. 2015. "Viral Activation of Stress-Regulated Rho-
745 GTPase Signaling Pathway Disrupts Sites of MRNA Degradation to Influence Cellular
746 Gene Expression." *Small GTPases* 6 (4): 178–85.
747 https://doi.org/10.1080/21541248.2015.1093068.

748 Cramer, Louise P., Margaret Siebert, and Timothy J. Mitchison. 1997. "Identification of Novel
749 Graded Polarity Actin Filament Bundles in Locomoting Heart Fibroblasts: Implications for
750 the Generation of Motile Force." *Journal of Cell Biology* 136 (6): 1287–1305.
751 https://doi.org/10.1083/jcb.136.6.1287.
752 Cuevas, Rolando A., Arundhati Ghosh, Christina Wallerath, Veit Hornung, Carolyn B. Coyne,
753 and Saumendra N. Sarkar. 2016. "MOV10 Provides Antiviral Activity against RNA Viruses
754 by Enhancing RIG-I–MAVS-Independent IFN Induction." *The Journal of Immunology* 196
755 (9): 3877–86. https://doi.org/10.4049/jimmunol.1501359.
756 Das, Joyjyoti, Somnath Maji, Tarun Agarwal, Suman Chakraborty, and Tapas K. Maiti. 2018.
757 "Hemodynamic Shear Stress Induces Protective Autophagy in HeLa Cells through Lipid
758 Raft-Mediated Mechanotransduction." *Clinical and Experimental Metastasis* 35 (3): 135–
759 48. https://doi.org/10.1007/s10585-018-9887-9.
760 Docena, G., L. Rovedatti, L. Kruidenier, Á Fanning, N. A.B. Leakey, C. H. Knowles, K. Lee, et
761 al. 2010. "Down-Regulation of P38 Mitogen-Activated Protein Kinase Activation and
762 Proinflammatory Cytokine Production by Mitogen-Activated Protein Kinase Inhibitors in
763 Inflammatory Bowel Disease." *Clinical and Experimental Immunology* 162 (1): 108–15.
764 https://doi.org/10.1111/j.1365-2249.2010.04203.x.
765 Dupont, Sirio, Leonardo Morsut, Mariaceleste Aragona, Elena Enzo, Stefano Giulitti,
766 Michelangelo Cordenonsi, Francesca Zanconato, et al. 2011. "Role of YAP/TAZ in
767 Mechanotransduction." *Nature* 474 (7350): 179–83. https://doi.org/10.1038/nature10137.
768 Edlund, Magnus, Marc A. Lotano, and Carol A. Otey. 2001. "Dynamics of Alpha-Actinin in
769 Focal Adhesions and Stress Fibers Visualized with Alpha-Actinin-Green Fluorescent
770 Protein." *Cell Motility and the Cytoskeleton* 48 (3): 190–200. https://doi.org/10.1002/1097-
771 0169(200103)48:3<190::AID-CM1008>3.0.CO;2-C.
772 Ensoli, B. 1998. "Kaposi's Sarcoma: A Result of the Interplay among Inflammatory Cytokines,
773 Angiogenic Factors and Viral Agents." *Cytokine & Growth Factor Reviews* 9 (1): 63–83.
774 https://doi.org/10.1016/S1359-6101(97)00037-3.
775 Eulalio, Ana, Isabelle Behm-Ansmant, and Elisa Izaurralde. 2007. "P Bodies: At the Crossroads
776 of Post-Transcriptional Pathways." *Nature Reviews Molecular Cell Biology* 8 (1): 9–22.
777 https://doi.org/10.1038/nrm2080.
778 Finch-Edmondson, Megan, and Marius Sudol. 2016. "Framework to Function: Mechanosensitive

779 Regulators of Gene Transcription." *Cellular & Molecular Biology Letters* 21 (1): 28.
780 https://doi.org/10.1186/s11658-016-0028-7.
781 Franks, Tobias M., and Jens Lykke-Andersen. 2007. "TTP and BRF Proteins Nucleate
782 Processing Body Formation to Silence MRNAs with AU-Rich Elements." *Genes and*
783 *Development* 21 (6): 719–35. https://doi.org/10.1101/gad.1494707.
784 Friedland, Julie C, Mark H Lee, and David Boettiger. 2009. "Mechanically Activated Integrin
785 Switch Controls Alpha5 Beta1 Function." *Science* 323 (January): 642–44.
786 Ganem, Don. 1997. "KSHV and Kaposi's Sarcoma: The End of the Beginning?" *Cell* 91 (2):
787 157–60. https://doi.org/10.1016/S0092-8674(00)80398-0.
788 Garcia, Melissa C., Denise M. Ray, Brad Lackford, Mark Rubino, Kenneth Olden, and John D.
789 Roberts. 2009. "Arachidonic Acid Stimulates Cell Adhesion through a Novel P38 MAPK-
790 RhoA Signaling Pathway That Involves Heat Shock Protein 27." *Journal of Biological*
791 *Chemistry* 284 (31): 20936–45. https://doi.org/10.1074/jbc.M109.020271.
792 Gomez-Garcia, M. Juliana, Amber L. Doiron, Robyn R. M. Steele, Hagar I. Labouta, Bahareh
793 Vafadar, Robert D. Shepherd, Ian D. Gates, David T. Cramb, Sarah J. Childs, and Kristina
794 D. Rinker. 2018. "Nanoparticle Localization in Blood Vessels: Dependence on Fluid Shear
795 Stress, Flow Disturbances, and Flow-Induced Changes in Endothelial Physiology."
796 *Nanoscale* 10 (32): 15249–61. https://doi.org/10.1039/C8NR03440K.
797 Grashoff, Carsten, Brenton D. Hoffman, Michael D. Brenner, Ruobo Zhou, Maddy Parsons,
798 Michael T. Yang, Mark A. McLean, et al. 2010. "Measuring Mechanical Tension across
799 Vinculin Reveals Regulation of Focal Adhesion Dynamics." *Nature* 466 (7303): 263–66.
800 https://doi.org/10.1038/nature09198.
801 Grossmann, Claudia, Simona Podgrabinska, Mihaela Skobe, and Don Ganem. 2006. "Activation
802 of NF-KB by the Latent VFLIP Gene of Kaposi's Sarcoma-Associated Herpesvirus Is
803 Required for the Spindle Shape of Virus-Infected Endothelial Cells and Contributes to Their
804 Proinflammatory Phenotype." *Journal of Virology* 80 (14): 7179–85.
805 https://doi.org/10.1128/jvi.01603-05.
806 Halder, Georg, Sirio Dupont, and Stefano Piccolo. 2012. "Transduction of Mechanical and
807 Cytoskeletal Cues by YAP and TAZ." *Nature Publishing Group* 13 (9): 591–600.
808 https://doi.org/10.1038/nrm3416.
809 Hardy, Shana D., Aparna Shinde, Wen Horng Wang, Michael K. Wendt, and Robert L. Geahlen.

2017. "Regulation of Epithelial-Mesenchymal Transition and Metastasis by TGF-β, P-Bodies, and Autophagy." *Oncotarget* 8 (61): 103302–14. https://doi.org/10.18632/oncotarget.21871.

Honda, K, T Yamada, R Endo, Y Ino, M Gotoh, H Tsuda, Y Yamada, H Chiba, and S Hirohashi. 1998. "Actinin-4, a Novel Actin-Bundling Protein Associated with Cell Motility and Cancer Invasion.[Erratum Appears in J Cell Biol 1998 Oct 5;143(1):Following 276]." *Journal of Cell Biology* 140 (6): 1383–93. https://doi.org/10.1083/jcb.140.6.1383.

Honda, Kazufumi. 2015. "The Biological Role of Actinin-4 (ACTN4) in Malignant Phenotypes of Cancer." *Cell and Bioscience* 5 (1): 1–9. https://doi.org/10.1186/s13578-015-0031-0.

Hotulainen, Pirta, and Pekka Lappalainen. 2006. "Stress Fibers Are Generated by Two Distinct Actin Assembly Mechanisms in Motile Cells." *Journal of Cell Biology* 173 (3): 383–94. https://doi.org/10.1083/jcb.200511093.

Huang, Yu, Li Wang, Jiang Yun Luo, Bochuan Li, Xiao Yu Tian, Li Jing Chen, Yuhong Huang, et al. 2016. "Integrin-YAP/TAZ-JNK Cascade Mediates Atheroprotective Effect of Unidirectional Shear Flow." *Nature* 540 (7634): 579–82. https://doi.org/10.1038/nature20602.

Ishizaki, T, M Uehata, I Tamechika, J Keel, K Nonomura, M Maekawa, and S Narumiya. 2000. "Pharmacological Properties of Y-27632, a Specific Inhibitor of Rho-Associated Kinases." *Molecular Pharmacology* 57 (5): 976–83. http://www.ncbi.nlm.nih.gov/pubmed/10779382.

Jackson, Wesley M., Michael J. Jaasma, Andrew D. Baik, and Tony M. Keaveny. 2008. "Over-Expression of Alpha-Actinin with a GFP Fusion Protein Is Sufficient to Increase Whole-Cell Stiffness in Human Osteoblasts." *Annals of Biomedical Engineering* 36 (10): 1605–14. https://doi.org/10.1007/s10439-008-9533-9.

Jang, Wonyul, Tackhoon Kim, Ja Seung Koo, Sang-kyum Kim, and Dae-Sik Lim. 2017. " Mechanical Cue-induced YAP Instructs Skp2-dependent Cell Cycle Exit and Oncogenic Signaling ." *The EMBO Journal* 36 (17): 2510–28. https://doi.org/10.15252/embj.201696089.

Joshi, Jyotsna, Gautam Mahajan, and Chandrasekhar R. Kothapalli. 2018. "Three-Dimensional Collagenous Niche and Azacytidine Selectively Promote Time-Dependent Cardiomyogenesis from Human Bone Marrow-Derived MSC Spheroids." *Biotechnology and Bioengineering* 115 (8): 2013–26. https://doi.org/10.1002/bit.26714.

841 Julian, Linda, and Michael F Olson. 2014. "Rho-Associated Coiled-Coil Containing Kinases
842 (ROCK)." *Small GTPases* 5 (2): e29846. https://doi.org/10.4161/sgtp.29846.
843 Kamentsky, Lee, Thouis R Jones, Adam Fraser, Mark-Anthony Bray, David J Logan, Katherine
844 L Madden, Vebjorn Ljosa, Curtis Rueden, Kevin W Eliceiri, and Anne E Carpenter. 2011.
845 "Improved Structure, Function and Compatibility for CellProfiler: Modular High-
846 Throughput Image Analysis Software." *Bioinformatics (Oxford, England)* 27 (8): 1179–80.
847 https://doi.org/10.1093/bioinformatics/btr095.
848 Kapoor, Avnish, Wantong Yao, Haoqiang Ying, Sujun Hua, Alison Liewen, Qiuyun Wang, Yi
849 Zhong, et al. 2014. "Yap1 Activation Enables Bypass of Oncogenic KRAS Addiction in
850 Pancreatic Cancer." *Cell* 158 (1): 185–97. https://doi.org/10.1016/j.cell.2014.06.003.
851 Katoh, K., Y. Kano, M. Masuda, H. Onishi, and K. Fujiwara. 1998. "Isolation and Contraction of
852 the Stress Fiber." *Molecular Biology of the Cell* 9 (7): 1919–38.
853 https://doi.org/10.1091/mbc.9.7.1919.
854 Kedersha, Nancy, and Paul Anderson. 2007. "Mammalian Stress Granules and Processing
855 Bodies." *Methods in Enzymology* 431 (07): 61–81. https://doi.org/10.1016/S0076-
856 6879(07)31005-7.
857 Kedersha, Nancy, Sarah Tisdale, Tyler Hickman, and Paul Anderson. 2008. *Chapter 26 Real-*
858 *Time and Quantitative Imaging of Mammalian Stress Granules and Processing Bodies*.
859 *Methods in Enzymology*. 1st ed. Vol. 448. Elsevier Inc. https://doi.org/10.1016/S0076-
860 6879(08)02626-8.
861 Kimura, K, M Ito, M Amano, K Chihara, Y Fukata, M Nakafuku, B Yamamori, et al. 1996.
862 "Regulation of Myosin Phosphatase by Rho and Rho-Associated Kinase (Rho-Kinase)."
863 *Science (New York, N.Y.)* 273 (5272): 245–48.
864 https://doi.org/10.1126/science.273.5272.245.
865 Kimura, Masahiro, Takahiro Horie, Osamu Baba, Yuya Ide, Shuhei Tsuji, Randolph Ruiz
866 Rodriguez, Toshimitsu Watanabe, et al. 2020. "Homeobox A4 Suppresses Vascular
867 Remodeling by Repressing YAP/TEAD Transcriptional Activity." *EMBO Reports* 21 (4):
868 e48389. https://doi.org/10.15252/embr.201948389.
869 Kong, Fang, Andrés J. García, A. Paul Mould, Martin J. Humphries, and Cheng Zhu. 2009.
870 "Demonstration of Catch Bonds between an Integrin and Its Ligand." *Journal of Cell*
871 *Biology* 185 (7): 1275–84. https://doi.org/10.1083/jcb.200810002.

872 Kovac, Bianca. 2010. "Role and Function of Nonmuscle Alpha-Actinin-1 and -4 in Regulating
873 Distinct Subcategories of Actin Stress Fibers in Mammalian Cells." University of Helsinki.
874 Kovacs, M., J. Toth, C. Hetenyi, A. Malnasi-Csizmadia, and J. R. Sellers. 2004. "Mechanism of
875 Blebbistatin Inhibition of Myosin II." *Journal of Biological Chemistry* 279 (34): 35557–63.
876 https://doi.org/10.1074/jbc.M405319200.
877 Lai, Jason Kuan Han, and Didier Y.R. Stainier. 2017. "Pushing Yap into the Nucleus with Shear
878 Force." *Developmental Cell* 40 (6): 517–18. https://doi.org/10.1016/j.devcel.2017.03.008.
879 Lazarides, Elias, and Keith Burridge. 1975. "α-Actinin: Immunofluorescent Localization of a
880 Muscle Structural Protein in Nonmuscle Cells." *Cell* 6 (3): 289–98.
881 https://doi.org/10.1016/0092-8674(75)90180-4.
882 Lee, Byoungkoo, Xin Zhou, Kristin Riching, Kevin W. Eliceiri, Patricia J. Keely, Scott A.
883 Guelcher, Alissa M. Weaver, and Yi Jiang. 2014. "A Three-Dimensional Computational
884 Model of Collagen Network Mechanics." Edited by Sanjay Kumar. *PLoS ONE* 9 (11):
885 e111896. https://doi.org/10.1371/journal.pone.0111896.
886 Lee, Hyun Jung, Miguel F. Diaz, Katherine M. Price, Joyce A. Ozuna, Songlin Zhang, Eva M.
887 Sevick-Muraca, John P. Hagan, and Pamela L. Wenzel. 2017. "Fluid Shear Stress Activates
888 YAP1 to Promote Cancer Cell Motility." *Nature Communications* 8 (1): 14122.
889 https://doi.org/10.1038/ncomms14122.
890 Lee, J. S. H. 2006. "Ballistic Intracellular Nanorheology Reveals ROCK-Hard Cytoplasmic
891 Stiffening Response to Fluid Flow." *Journal of Cell Science* 119 (9): 1760–68.
892 https://doi.org/10.1242/jcs.02899.
893 Lee, Stacey, and Sanjay Kumar. 2016. "Actomyosin Stress Fiber Mechanosensing in 2D and
894 3D." *F1000Research* 5 (0): 2261. https://doi.org/10.12688/f1000research.8800.1.
895 Li, Ying, Rui Chen, Qian Zhou, Zhisheng Xu, Chao Li, Shuai Wang, Aiping Mao, Xiaodong
896 Zhang, Weiwu He, and Hong Bing Shu. 2012. "LSm14A Is a Processing Body-Associated
897 Sensor of Viral Nucleic Acids That Initiates Cellular Antiviral Response in the Early Phase
898 of Viral Infection." *Proceedings of the National Academy of Sciences of the United States of*
899 *America* 109 (29): 11770–75. https://doi.org/10.1073/pnas.1203405109.
900 Liu, G., F. X. Yu, Y. C. Kim, Z. Meng, J. Naipauer, D. J. Looney, X. Liu, J. S. Gutkind, E. A.
901 Mesri, and K. L. Guan. 2015. "Kaposi Sarcoma-Associated Herpesvirus Promotes
902 Tumorigenesis by Modulating the Hippo Pathway." *Oncogene* 34 (27): 3536–46.

https://doi.org/10.1038/onc.2014.281.

Liu, Huan, Xiaoming Dai, Xiaolei Cao, Huan Yan, Xinyan Ji, Haitao Zhang, Shuying Shen, et al. 2018. "PRDM4 Mediates YAP-induced Cell Invasion by Activating Leukocyte-specific Integrin B2 Expression." *EMBO Reports* 19 (6): 1–14. https://doi.org/10.15252/embr.201745180.

Liu, J., X. Bi, T. Chen, Q. Zhang, S. X. Wang, J. J. Chiu, G. S. Liu, Y. Zhang, P. Bu, and F. Jiang. 2015. "Shear Stress Regulates Endothelial Cell Autophagy via Redox Regulation and Sirt1 Expression." *Cell Death and Disease* 6 (7). https://doi.org/10.1038/cddis.2015.193.

Liu, Zeming, Wen Zeng, Shi Wang, Xiangwang Zhao, Yawen Guo, Pan Yu, Xingjie Yin, Chunping Liu, and Tao Huang. 2017. "A Potential Role for the Hippo Pathway Protein, YAP, in Controlling Proliferation, Cell Cycle Progression, and Autophagy in BCPAP and KI Thyroid Papillary Carcinoma Cells." *American Journal of Translational Research* 9 (7): 3212–23.

Lumb, Jennifer H., Lauren M. Popov, Siyuan Ding, Marie T. Keith, Bryan D. Merrill, Harry B. Greenberg, Jan E. Carette, Qin Li, and Jin Billy Li. 2017. "DDX6 Represses Aberrant Activation of Interferon-Stimulated Genes." *Cell Reports* 20 (4): 819–31. https://doi.org/10.1016/j.celrep.2017.06.085.

McCormick, Craig, and Don Ganem. 2005. "The Kaposin B Protein of KSHV Activates the P38/MK2 Pathway and Stabilizes Cytokine MRNAs." *Science* 307 (5710): 739–41. https://doi.org/10.1126/science.1105779.

Montaner, Silvia, Akrit Sodhi, Amanda K. Ramsdell, Daniel Martin, Jiadi Hu, Earl T. Sawai, and J. Silvio Gutkind. 2006. "The Kaposi's Sarcoma-Associated Herpesvirus G Protein-Coupled Receptor as a Therapeutic Target for the Treatment of Kaposi's Sarcoma." *Cancer Research* 66 (1): 168–74. https://doi.org/10.1158/0008-5472.CAN-05-1026.

Moreno-Vicente, Roberto, Dácil María Pavón, Inés Martín-Padura, Mauro Català-Montoro, Alberto Díez-Sánchez, Antonio Quílez-Álvarez, Juan Antonio López, et al. 2018. "Caveolin-1 Modulates Mechanotransduction Responses to Substrate Stiffness through Actin-Dependent Control of YAP." *Cell Reports* 25 (6): 1622-1635.e6. https://doi.org/10.1016/j.celrep.2018.10.024.

Nakajima, Hiroyuki, and Naoki Mochizuki. 2017. "Flow Pattern-Dependent Endothelial Cell Responses through Transcriptional Regulation." *Cell Cycle* 16 (20): 1893–1901.

https://doi.org/10.1080/15384101.2017.1364324.

Nakajima, Hiroyuki, Kimiko Yamamoto, Sobhika Agarwala, Kenta Terai, Hajime Fukui, Shigetomo Fukuhara, Koji Ando, et al. 2017. "Flow-Dependent Endothelial YAP Regulation Contributes to Vessel Maintenance." *Developmental Cell* 40 (6): 523-536.e6. https://doi.org/10.1016/j.devcel.2017.02.019.

Naranatt, Pramod P., Shaw M. Akula, Christopher A. Zien, Harinivas H. Krishnan, and Bala Chandran. 2003. "Kaposi's Sarcoma-Associated Herpesvirus Induces the Phosphatidylinositol 3-Kinase-PKC-ζ-MEK-ERK Signaling Pathway in Target Cells Early during Infection: Implications for Infectivity." *Journal of Virology* 77 (2): 1524–39. https://doi.org/10.1128/jvi.77.2.1524-1539.2003.

Ng, Chen Seng, Dacquin M. Kasumba, Takashi Fujita, and Honglin Luo. 2020. "Spatio-Temporal Characterization of the Antiviral Activity of the XRN1-DCP1/2 Aggregation against Cytoplasmic RNA Viruses to Prevent Cell Death." *Cell Death and Differentiation*. https://doi.org/10.1038/s41418-020-0509-0.

Noria, Sabrena, Feng Xu, Shannon McCue, Mara Jones, Avrum I Gotlieb, and B Lowell Langille. 2004. "Assembly and Reorientation of Stress Fibers Drives Morphological Changes to Endothelial Cells Exposed to Shear Stress." *The American Journal of Pathology* 164 (4): 1211–23. https://doi.org/10.1016/S0002-9440(10)63209-9.

Núñez, Rocío Daviña, Matthias Budt, Sandra Saenger, Katharina Paki, Ulrike Arnold, Anne Sadewasser, and Thorsten Wolff. 2018. "The RNA Helicase DDX6 Associates with RIG-I to Augment Induction of Antiviral Signaling." *International Journal of Molecular Sciences* 19 (7): 1–14. https://doi.org/10.3390/ijms19071877.

Ohashi, Kazumasa, Kyoko Nagata, Midori Maekawa, Toshimasa Ishizaki, Shuh Narumiya, and Kensaku Mizuno. 2000. "Rho-Associated Kinase ROCK Activates LIM-Kinase 1 by Phosphorylation at Threonine 508 within the Activation Loop." *Journal of Biological Chemistry* 275 (5): 3577–82. https://doi.org/10.1074/jbc.275.5.3577.

Ojala, Päivi M., and Thomas F. Schulz. 2014. "Manipulation of Endothelial Cells by KSHV: Implications for Angiogenesis and Aberrant Vascular Differentiation." *Seminars in Cancer Biology* 26 (June): 69–77. https://doi.org/10.1016/j.semcancer.2014.01.008.

Ostareck, Dirk H., Isabel S. Naarmann-de Vries, and Antje Ostareck-Lederer. 2014. "DDX6 and Its Orthologs as Modulators of Cellular and Viral RNA Expression." *Wiley Interdisciplinary*

Reviews: RNA 5 (5): 659–78. https://doi.org/10.1002/wrna.1237.

Panciera, Tito, Luca Azzolin, Atsushi Fujimura, Daniele Di Biagio, Chiara Frasson, Silvia Bresolin, Sandra Soligo, et al. 2016. "Induction of Expandable Tissue-Specific Stem/Progenitor Cells through Transient Expression of YAP/TAZ." *Cell Stem Cell* 19 (6): 725–37. https://doi.org/10.1016/j.stem.2016.08.009.

Pei, Tianjiao, Xin Huang, Ying Long, Changling Duan, Tingting Liu, Yujing Li, and Wei Huang. 2019. "Increased Expression of YAP Is Associated with Decreased Cell Autophagy in the Eutopic Endometrial Stromal Cells of Endometriosis." *Molecular and Cellular Endocrinology* 491 (April): 110432. https://doi.org/10.1016/j.mce.2019.04.012.

Pellegrin, S., and H. Mellor. 2007. "Actin Stress Fibres." *Journal of Cell Science* 120 (20): 3491–99. https://doi.org/10.1242/jcs.018473.

Pollard, Thomas D. 2016. "Actin and Actin-Binding Proteins." *Cold Spring Harbor Perspectives in Biology* 8 (8): a018226. https://doi.org/10.1101/cshperspect.a018226.

Rasmussen, Izabela, Line H Pedersen, Luise Byg, Kazuhiro Suzuki, Hideki Sumimoto, and Frederik Vilhardt. 2010. "Effects of F/G-Actin Ratio and Actin Turn-over Rate on NADPH Oxidase Activity in Microglia." *BMC Immunology* 11 (1): 44. https://doi.org/10.1186/1471-2172-11-44.

Ridley, Anne J., and Alan Hall. 1992. "The Small GTP-Binding Protein Rho Regulates the Assembly of Focal Adhesions and Actin Stress Fibers in Response to Growth Factors." *Cell* 70 (3): 389–99. https://doi.org/10.1016/0092-8674(92)90163-7.

Rio, Armando del, Raul Perez-jimenez, Ruchuan Liu, Pere Roca-cusachs, Julio M Fernandez, and Michael P Sheetz. 2009. "Stretching Single Talin Rod." *Science* 323 (5914): 638–41.

Rotsch, Christian, and Manfred Radmacher. 2000. "Drug-Induced Changes of Cytoskeletal Structure and Mechanics in Fibroblasts: An Atomic Force Microscopy Study." *Biophysical Journal* 78 (1): 520–35. https://doi.org/10.1016/S0006-3495(00)76614-8.

Russo, James J, Roy A Bohenzky, M.-C. Chien, Jing Chen, Ming Yan, Dawn Maddalena, J Preston Parry, et al. 1996. "Nucleotide Sequence of the Kaposi Sarcoma-Associated Herpesvirus (HHV8)." *Proceedings of the National Academy of Sciences* 93 (25): 14862–67. https://doi.org/10.1073/pnas.93.25.14862.

Schmitz, Arndt A.P., Eve-Ellen Govek, Benjamin Böttner, and Linda Van Aelst. 2000. "Rho GTPases: Signaling, Migration, and Invasion." *Experimental Cell Research* 261 (1): 1–12.

https://doi.org/10.1006/excr.2000.5049.

Sharma, Nishi R, Vladimir Majerciak, Michael J Kruhlak, Lulu Yu, Jeong Gu Kang, Acong Yang, Shuo Gu, Marvin J Fritzler, and Zhi-ming Zheng. 2019. "KSHV RNA-Binding Protein ORF57 Inhibits P-Body Formation to Promote Viral Multiplication by Interaction with Ago2 and GW182," 1–18. https://doi.org/10.1093/nar/gkz683.

Shaw, Gray, and Robert Kamen. 1986. "A Conserved AU Sequence from the 3′ Untranslated Region of GM-CSF MRNA Mediates Selective MRNA Degradation." *Cell* 46 (5): 659–67. https://doi.org/10.1016/0092-8674(86)90341-7.

Shen, Zhewei, and Ben Z. Stanger. 2015. "YAP Regulates S-Phase Entry in Endothelial Cells." Edited by Deanna M Koepp. *PLOS ONE* 10 (1): e0117522. https://doi.org/10.1371/journal.pone.0117522.

Sheth, Ujwal. 2003. "Decapping and Decay of Messenger RNA Occur in Cytoplasmic Processing Bodies." *Science* 300 (5620): 805–8. https://doi.org/10.1126/science.1082320.

Shyu, A. B., M. E. Greenberg, and J. G. Belasco. 1989. "The C-Fos Transcript Is Targeted for Rapid Decay by Two Distinct MRNA Degradation Pathways." *Genes & Development* 3 (1): 60–72. https://doi.org/10.1101/gad.3.1.60.

Small, J. Victor, K. Rottner, I. Kaverina, and K. I. Anderson. 1998. "Assembling an Actin Cytoskeleton for Cell Attachment and Movement." *Biochimica et Biophysica Acta - Molecular Cell Research* 1404 (3): 271–81. https://doi.org/10.1016/S0167-4889(98)00080-9.

Song, Qinghe, Beibei Mao, Jinbo Cheng, Yuhao Gao, Ke Jiang, Jun Chen, Zengqiang Yuan, and Songshu Meng. 2015. "YAP Enhances Autophagic Flux to Promote Breast Cancer Cell Survival in Response to Nutrient Deprivation." *PLoS ONE* 10 (3). https://doi.org/10.1371/journal.pone.0120790.

Sotiropoulos, Athanassia, Dziugas Gineitis, John Copeland, and Richard Treisman. 1999. "Signal-Regulated Activation of Serum Response Factor Is Mediated by Changes in Actin Dynamics." *Cell* 98 (2): 159–69. https://doi.org/10.1016/S0092-8674(00)81011-9.

Speck, Samuel H., and Don Ganem. 2010. "Viral Latency and Its Regulation: Lessons from the γ-Herpesviruses." *Cell Host and Microbe* 8 (1): 100–115. https://doi.org/10.1016/j.chom.2010.06.014.

Staskus, K A, W Zhong, K Gebhard, B Herndier, H Wang, R Renne, J Beneke, et al. 1997.

"Kaposi's Sarcoma-Associated Herpesvirus Gene Expression in Endothelial (Spindle) Tumor Cells." *Journal of Virology* 71 (1): 715–19. https://doi.org/10.1128/jvi.71.1.715-719.1997.

Stoecklin, Georg, Thomas Mayo, and Paul Anderson. 2006. "ARE-MRNA Degradation Requires the 5'-3' Decay Pathway." *EMBO Reports* 7 (1): 72–77. https://doi.org/10.1038/sj.embor.7400572.

Sugimoto, Wataru, Katsuhiko Itoh, Yasumasa Mitsui, Takahiro Ebata, Hideaki Fujita, Hiroaki Hirata, and Keiko Kawauchi. 2018. "Substrate Rigidity-Dependent Positive Feedback Regulation between YAP and ROCK2." *Cell Adhesion and Migration* 12 (2): 101–8. https://doi.org/10.1080/19336918.2017.1338233.

Takahashi, Shinya, Kyoko Sakurai, Arisa Ebihara, Hiroaki Kajiho, Kota Saito, Kenji Kontani, Hiroshi Nishina, and Toshiaki Katada. 2011. "RhoA Activation Participates in Rearrangement of Processing Bodies and Release of Nucleated AU-Rich MRNAs." *Nucleic Acids Research* 39 (8): 3446–57. https://doi.org/10.1093/nar/gkq1302.

Tan, John L, Joe Tien, Dana M Pirone, Darren S Gray, Kiran Bhadriraju, and Christopher S Chen. 2003. "Cells Lying on a Bed of Microneedles: An Approach to Isolate Mechanical Force." *Proceedings of the National Academy of Sciences* 100 (4): 1484–89. https://doi.org/10.1073/pnas.0235407100.

Tojkander, Sari, Gergana Gateva, and Pekka Lappalainen. 2012. "Actin Stress Fibers - Assembly, Dynamics and Biological Roles." *Journal of Cell Science* 125 (Pt 8): 1855–64. https://doi.org/10.1242/jcs.098087.

Totaro, Antonio, Qiuyu Zhuang, Tito Panciera, Giusy Battilana, Luca Azzolin, Giulia Brumana, Alessandro Gandin, Giovanna Brusatin, Michelangelo Cordenonsi, and Stefano Piccolo. 2019. "Cell Phenotypic Plasticity Requires Autophagic Flux Driven by YAP/TAZ Mechanotransduction." *Proceedings of the National Academy of Sciences* 116 (36): 17848–57. https://doi.org/10.1073/pnas.1908228116.

Umbach, Jennifer L., Hui Ling Yen, Leo L M Poon, and Bryan R. Cullen. 2010. "Influenza a Virus Expresses High Levels of an Unusual Class of Small Viral Leader RNAs in Infected Cells." *MBio* 1 (4): 1–8. https://doi.org/10.1128/mBio.00204-10.

Vallenius, Tea. 2013. "Actin Stress Fibre Subtypes in Mesenchymal-Migrating Cells." *Open Biology* 3 (6): 130001. https://doi.org/10.1098/rsob.130001.

Vassilev, Alex, Kotaro J. Kaneko, Hongjun Shu, Yingming Zhao, and Melvin L. DePamphilis. 2001. "TEAD/TEF Transcription Factors Utilize the Activation Domain of YAP65, a Src/Yes-Associated Protein Localized in the Cytoplasm." *Genes and Development* 15 (10): 1229–41. https://doi.org/10.1101/gad.888601.

Vindry, Caroline, Aline Marnef, Helen Broomhead, Laure Twyffels, Sevim Ozgur, Georg Stoecklin, Miriam Llorian, et al. 2017. "Dual RNA Processing Roles of Pat1b via Cytoplasmic Lsm1-7 and Nuclear Lsm2-8 Complexes." *Cell Reports* 20 (5): 1187–1200. https://doi.org/10.1016/j.celrep.2017.06.091.

Vozzi, Federico, Jonica Campolo, Lorena Cozzi, Gianfranco Politano, Stefano Di Carlo, Michela Rial, Claudio Domenici, and Oberdan Parodi. 2018. "Computing of Low Shear Stress-Driven Endothelial Gene Network Involved in Early Stages of Atherosclerotic Process." *BioMed Research International* 2018 (September): 1–12. https://doi.org/10.1155/2018/5359830.

Wada, K.-I., K. Itoga, T. Okano, S. Yonemura, and H. Sasaki. 2011. "Hippo Pathway Regulation by Cell Morphology and Stress Fibers." *Development* 138 (18): 3907–14. https://doi.org/10.1242/dev.070987.

Wakatsuki, T, B Schwab, N Thompson, and EL Elson. 2001. "Effects of Cytochalasin D and Latrunculin B on Mechanical Properties of Cells." *Journal of Cell Science* 114 (5): 1025–36.

Wang, Huanru, Liang Chang, Xiaohui Wang, Airong Su, Chunhong Feng, Yuxuan Fu, Deyan Chen, Nan Zheng, and Zhiwei Wu. 2016. "MOV10 Interacts with Enterovirus 71 Genomic 5′UTR and Modulates Viral Replication." *Biochemical and Biophysical Research Communications* 479 (3): 571–77. https://doi.org/10.1016/j.bbrc.2016.09.112.

Wang, Kuei-Chun, Yi-Ting Yeh, Phu Nguyen, Elaine Limqueco, Jocelyn Lopez, Satenick Thorossian, Kun-Liang Guan, Yi-Shuan J. Li, and Shu Chien. 2016. "Flow-Dependent YAP/TAZ Activities Regulate Endothelial Phenotypes and Atherosclerosis." *Proceedings of the National Academy of Sciences* 113 (41): 11525–30. https://doi.org/10.1073/pnas.1613121113.

Wang, Xiaoli, Yingying Zhang, Tang Feng, Guanyue Su, Jia He, Wenbo Gao, Yang Shen, and Xiaoheng Liu. 2018. "Fluid Shear Stress Promotes Autophagy in Hepatocellular Carcinoma Cells." *International Journal of Biological Sciences* 14 (10): 1277–90.

https://doi.org/10.7150/ijbs.27055.

Watanabe, Naoki, Takayuki Kato, Akiko Fujita, Toshimasa Ishizaki, and Shuh Narumiya. 1999. "Cooperation between MDia1 and ROCK in Rho-Induced Actin Reorganization." *Nature Cell Biology* 1 (3): 136–43. https://doi.org/10.1038/11056.

Watanabe, Naoki, Pascal Madaule, Tim Reid, Toshimasa Ishizaki, Go Watanabe, Akira Kakizuka, Yuji Saito, Kazuwa Nakao, Brigitte M. Jockusch, and Shuh Narumiya. 1997. "P140mDia, a Mammalian Homolog of Drosophila Diaphanous, Is a Target Protein for Rho Small GTPase and Is a Ligand for Profilin." *EMBO Journal* 16 (11): 3044–56. https://doi.org/10.1093/emboj/16.11.3044.

Winzen, Reinhard, Michael Kracht, Birgit Ritter, Arno Wilhelm, Chyi Ying A. Chen, Ann Bin Shyu, Monika Müller, Matthias Gaestel, Klaus Resch, and Helmut Holtmann. 1999. "The P38 MAP Kinase Pathway Signals for Cytokine-Induced MRNA Stabilization via MAP Kinase-Activated Protein Kinase 2 and an AU-Rich Region-Targeted Mechanism." *EMBO Journal* 18 (18): 4969–80. https://doi.org/10.1093/emboj/18.18.4969.

Yang, Chih-Sheng, Eleni Stampouloglou, Nathan M Kingston, Liye Zhang, Stefano Monti, and Xaralabos Varelas. 2018. "Glutamine-utilizing Transaminases Are a Metabolic Vulnerability of TAZ/YAP-activated Cancer Cells." *EMBO Reports* 19 (6): 1–11. https://doi.org/10.15252/embr.201643577.

Yang, Ya Li, Lindsay M. Leone, and Laura J. Kaufman. 2009. "Elastic Moduli of Collagen Gels Can Be Predicted from Two-Dimensional Confocal Microscopy." *Biophysical Journal* 97 (7): 2051–60. https://doi.org/10.1016/j.bpj.2009.07.035.

Yao, Pingbo, Hong Zhao, Wenjuan Mo, and Pingping He. 2015. "Laminar Shear Stress Promotes Vascular Endothelial Cell Autophagy Through Upregulation with Rab4." *DNA and Cell Biology* 35 (3): 118–23. https://doi.org/10.1089/dna.2015.3041.

Yu, Fa Xing, Bin Zhao, Nattapon Panupinthu, Jenna L. Jewell, Ian Lian, Lloyd H. Wang, Jiagang Zhao, et al. 2012. "Regulation of the Hippo-YAP Pathway by G-Protein-Coupled Receptor Signaling." *Cell* 150 (4): 780–91. https://doi.org/10.1016/j.cell.2012.06.037.

Yu, Jiang Hong, Wei-Hong Yang, Tod Gulick, Kenneth D Bloch, and Donald B Bloch. 2005. "Ge-1 Is a Central Component of the Mammalian Cytoplasmic MRNA Processing Body." *RNA (New York, N.Y.)* 11 (12): 1795–1802. https://doi.org/10.1261/rna.2142405.

Zanconato, Francesca, Mattia Forcato, Giusy Battilana, Luca Azzolin, Erika Quaranta, Beatrice

Bodega, Antonio Rosato, Silvio Bicciato, Michelangelo Cordenonsi, and Stefano Piccolo. 2015. "Genome-Wide Association between YAP/TAZ/TEAD and AP-1 at Enhancers Drives Oncogenic Growth." *Nature Cell Biology* 17 (9): 1218–27. https://doi.org/10.1038/ncb3216.

Zhang, Qian, Fansen Meng, Shasha Chen, Steven W Plouffe, Shiying Wu, Shengduo Liu, Xinran Li, et al. 2017. "Hippo Signalling Governs Cytosolic Nucleic Acid Sensing through YAP / TAZ-Mediated TBK1 Blockade." *Nature Cell Biology* 19 (4): 362–74. https://doi.org/10.1038/ncb3496.

Zhao, Bin, Li Li, Lloyd Wang, Cun Yu Wang, Jindan Yu, and Kun Liang Guan. 2012. "Cell Detachment Activates the Hippo Pathway via Cytoskeleton Reorganization to Induce Anoikis." *Genes and Development* 26 (1): 54–68. https://doi.org/10.1101/gad.173435.111.

Zhao, Bin, Bin Zhao, Xiaomu Wei, Xiaomu Wei, Weiquan Li, Weiquan Li, Ryan S Udan, et al. 2007. "Inactivation of YAP Oncoprotein by the Hippo Pathway Is Involved in Cell Contact Inhibition and Tissue Growth Control." *Genes and Development* 21: 2747–61. https://doi.org/10.1101/gad.1602907.Hpo/Sav.

Zhong, W, H Wang, B Herndier, and D Ganem. 1996. "Restricted Expression of Kaposi Sarcoma-Associated Herpesvirus (Human Herpesvirus 8) Genes in Kaposi Sarcoma." *Proceedings of the National Academy of Sciences of the United States of America* 93 (13): 6641–46. https://doi.org/10.1073/pnas.93.13.6641.

Acknowledgements

We would like to sincerely thank the members of the Corcoran lab for helpful discussions about this work, notably Carolyn-Ann Robinson. We would like to thank Dr. Craig McCormick (Dalhousie University) and his lab for plasmids, expertise and invaluable advice. ELC was supported by a Killam predoctoral scholarship, an NSERC CGS-M scholarship, and a Nova Scotia Graduate scholarship. Operating funds to support this work derive from an NSERC Discovery grant RGPIN-2015-04882 to JAC.

Competing Interests

The authors have no competing interests to declare.

Author Contributions

Elizabeth L. Castle: Conceptualization, Experimentation, Analysis, Paper Writing

Dr. Pauline Douglas: Experimentation

Dr. Kristina Rinker: Conceptualization

Dr. Jennifer A. Corcoran: Conceptualization, Experimentation, Supervision, Funding Acquisition, Project Administration, Paper Writing

Figures

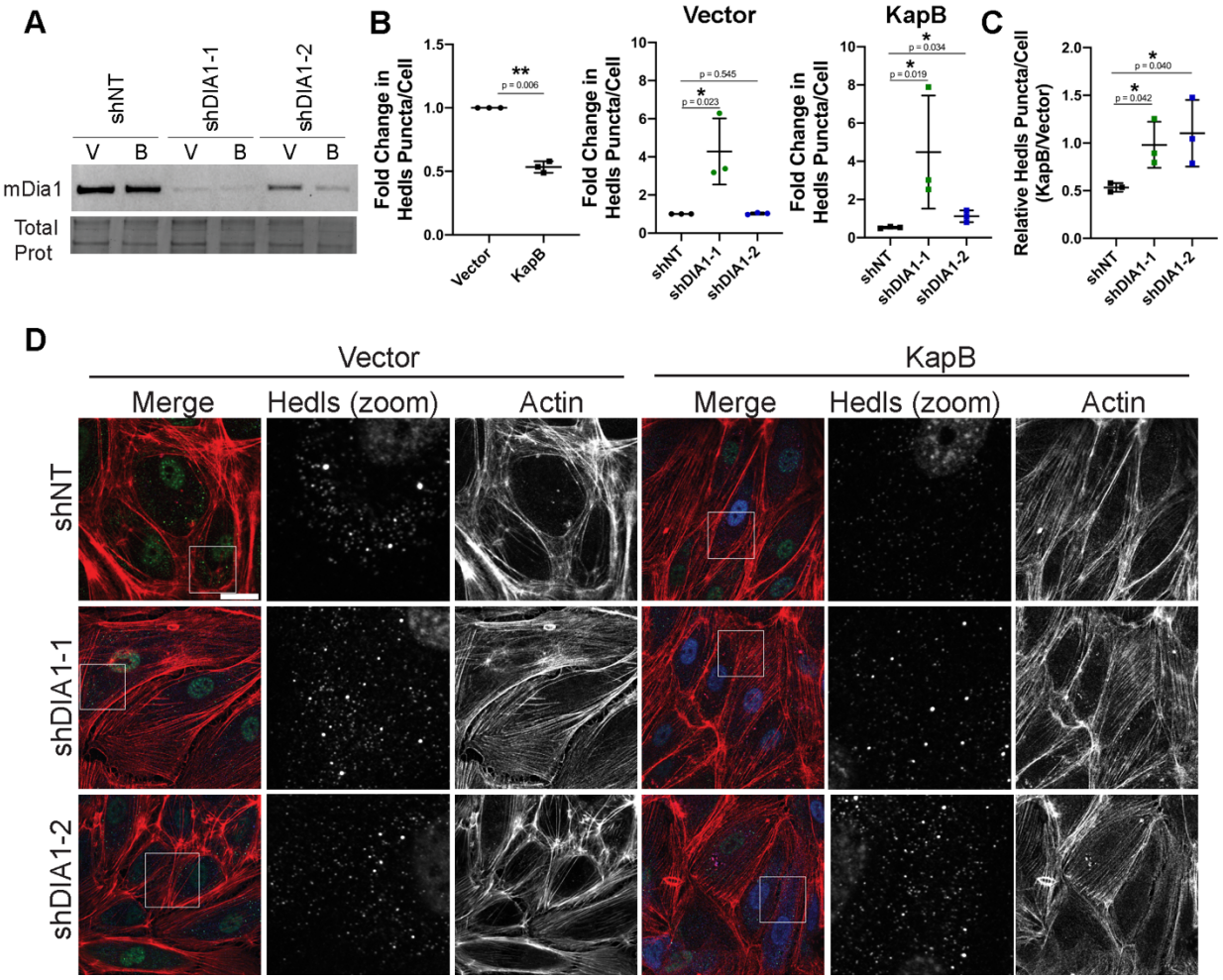

Figure 1: The RhoA-effector mDia1 is required for KapB-mediated PB disassembly. KapB- and vector- expressing HUVECs were transduced with shRNAs targeting mDia1 (shDIA1-1, shDIA1-2) or with a non-targeting (shNT) control and selected. In parallel, cells were fixed for immunofluorescence or lysed for immunoblotting. (A) One representative immunoblot of three independent experiments stained with mDia1-specific antibody is shown. (B, C) Fixed cells were stained for CellProfiler analysis as detailed in the methods. (B) The number of Hedls puncta per cell was quantified and normalized to the vector NT control within each replicate. (C) CellProfiler data was used to calculate the ratio of Hedls puncta counts in KapB-expressing cells versus the vector control for each treatment condition. (D) Representative images of cells stained for PB-resident protein Hedls (green), KapB (blue), and F-actin (red, phalloidin). Boxes indicate area shown in the Hedls (zoom) panel. Scale bar represents 20 μm. Statistics were determined using ratio paired t-tests between control and experimental groups; error bars represent standard deviation; n=3 independent biological replicates; * = $p < 0.05$, ** = $p < 0.01$.

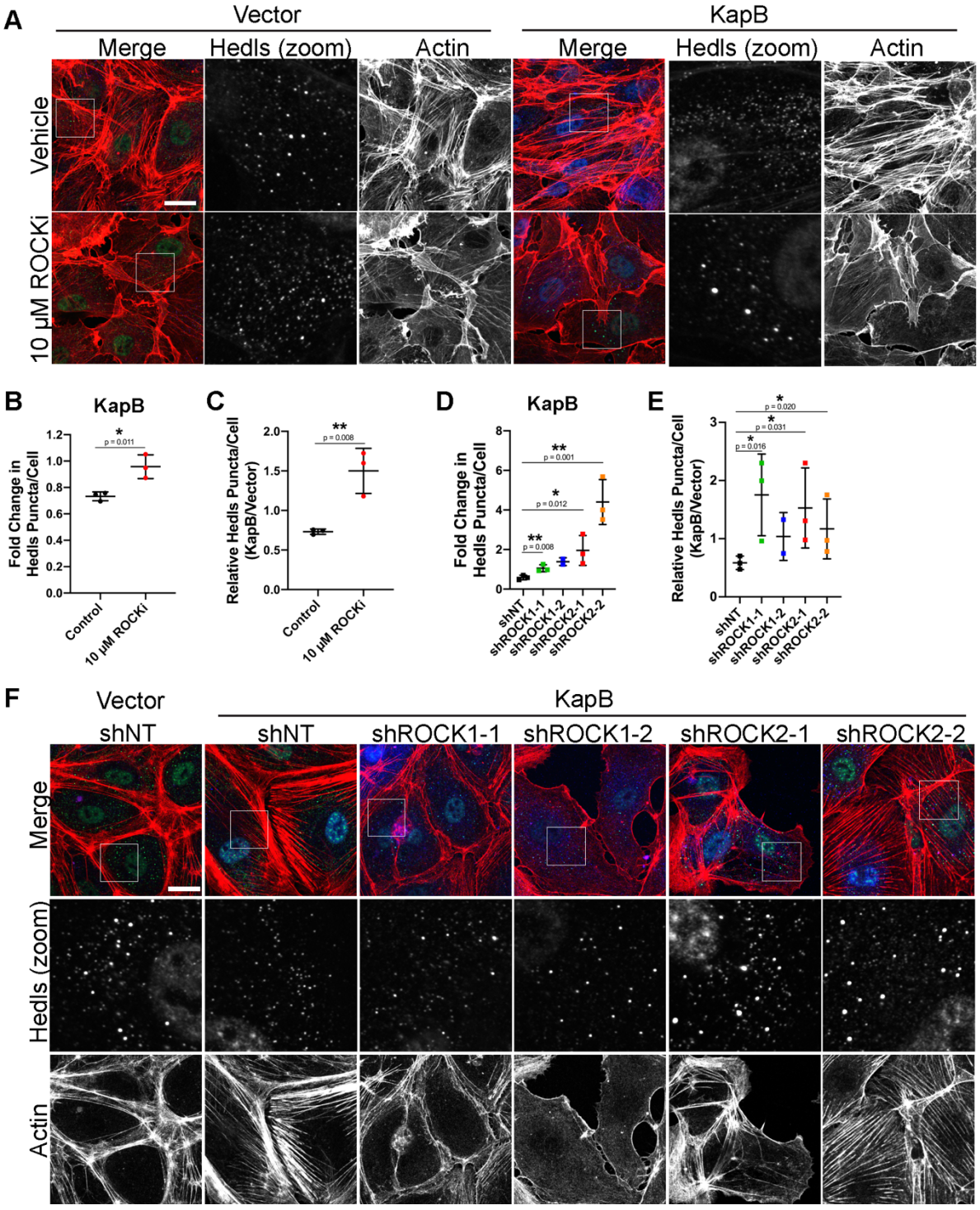

Figure 2: The RhoA-effector ROCK is required for KapB-mediated PB disassembly. (A-C) KapB- and vector- expressing HUVECs were treated with 10 ⌈M Y-27632 or water control for 4 h and fixed for immunofluorescence. (A) Representative images of cells stained for PB-resident protein Hedls (green), KapB (blue), and F-actin (red, phalloidin). Boxes indicate area shown in the Hedls (zoom) panel. Scale bar represents 20 μm. (B, C) Fixed cells were stained for CellProfiler analysis as detailed in the methods. (B) The number of Hedls puncta per cell was

quantified and normalized to the vector NT control within each replicate. (C) CellProfiler data was used to calculate the ratio of Hedls puncta counts in KapB-expressing cells versus the vector control for each treatment condition. (D-F) KapB- and vector- expressing HUVECs were transduced with shRNAs targeting ROCK1 and ROCK2 (shROCK1-1, shROCK1-2, shROCK2-1, shROCK2-2) or with a non-targeting (shNT) control and selected. Cells were fixed for immunofluorescence. (D, E) Fixed cells were stained for CellProfiler analysis as detailed in the methods. (D) The number of Hedls puncta per cell was quantified and normalized to the vector NT control within each replicate. (E) CellProfiler data was used to calculate the ratio of Hedls puncta counts in KapB-expressing cells versus the vector control for each treatment condition. (F) Representative images of cells stained for PB-resident protein Hedls (green), KapB (blue), and F-actin (red, phalloidin). Boxes indicate images shown in Hedls (zoom) panel. Scale bar represents 20 μm. Statistics were determined using ratio paired t-tests between control and experimental groups; error bars represent standard deviation from n=3 independent biological replicates except shROCK1-2, (n=2); * = $p < 0.05$, ** = $p < 0.01$.

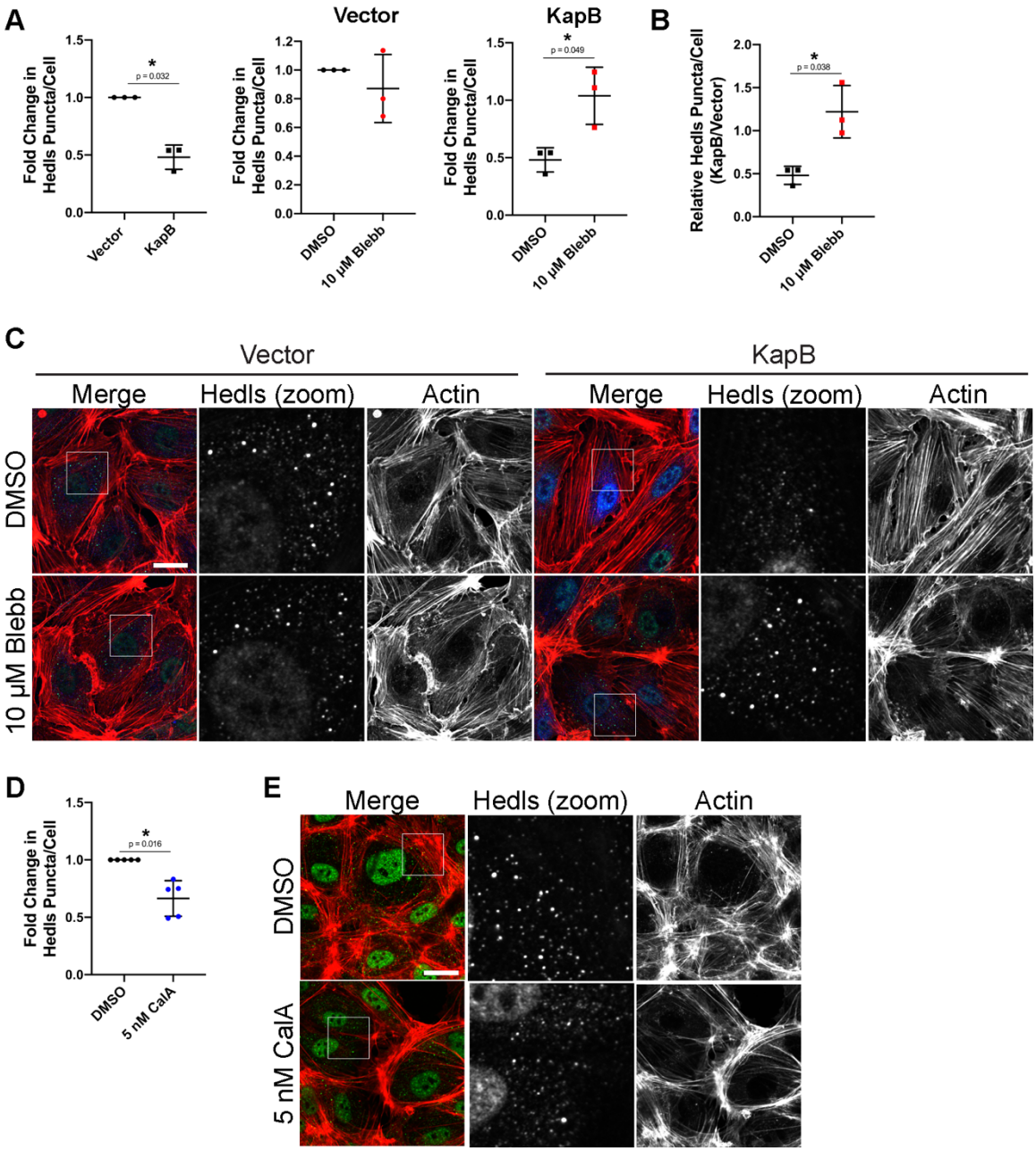

Figure 3: Actomyosin contractility controls PB disassembly. (A-C) KapB- and vector-expressing HUVECs were treated with 10 ⌈M blebbistatin to inhibit actomyosin contractility or DMSO for 30 min and fixed for immunofluorescence. (A, B) Fixed cells were stained for CellProfiler analysis as detailed in the methods. (A) The number of Hedls puncta per cell was quantified and normalized to the vector NT control within each replicate. (B) CellProfiler data was used to calculate the ratio of Hedls puncta counts in KapB-expressing cells versus the vector control for each treatment condition. (C) Representative images of cells stained for PB-resident protein Hedls (green), KapB (blue), and F-actin (red, phalloidin). Boxes indicate area shown in the Hedls (zoom) panel. Scale bar represents 20 μm. (D, E) Untransduced HUVECs were treated with 5 nM Calyculin A (CalA) to stimulate actomyosin contraction or DMSO for 20 min and fixed for immunofluorescence. (D) Fixed cells were stained for CellProfiler analysis as detailed

in the methods. Hedls puncta per cell were quantified and normalized to the DMSO control within each replicate. (E) Representative images of cells treated with 5 nM CalA and stained for PB-resident protein Hedls (green) and F-actin (red, phalloidin). Boxes indicate area shown in the Hedls (zoom) panel. Scale bar represents 20 μm. Statistics were determined using ratio paired t-tests between control and experimental groups; error bars represent standard deviation; n=3 (A, B) and n=5 (D) independent biological replicates; * = $p < 0.05$.

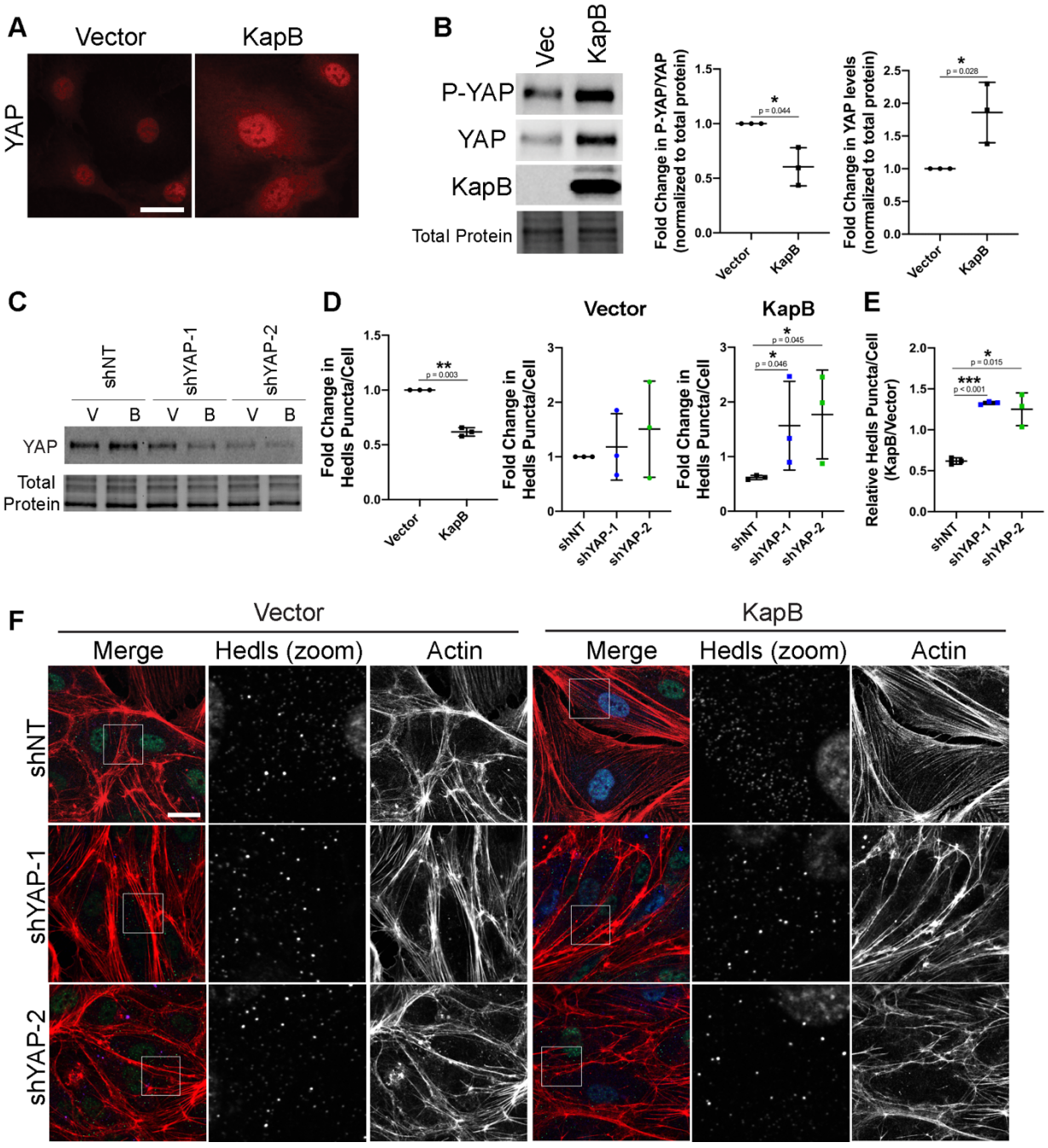

Figure 4: YAP is required for KapB-mediated PB disassembly. (A, B) KapB- and vector-expressing HUVECs were fixed for immunofluorescence or lysed for immunoblotting. (A) Representative images of cells stained for YAP (red). Scale bar represents 20 μM. (B) One representative immunoblot and quantification of three independent experiments stained with P(S127)-YAP-, YAP- or KapB-specific antibody are shown. Protein levels in each condition were normalized to total protein. All treatments were normalized to vector control within each replicate. (C-F) KapB- and vector- expressing HUVECs were transduced with shRNAs targeting YAP (shYAP-1, shYAP-2) or with a non-targeting (shNT) control and selected. In parallel, cells were fixed for immunofluorescence or lysed for immunoblotting. (C) One representative

immunoblot of three independent experiments stained with YAP-specific antibody is shown. (D, E) Fixed cells were stained for CellProfiler analysis as detailed in the methods. (D) The number of Hedls puncta per cell was quantified and normalized to the vector NT control within each replicate. (E) CellProfiler data was used to calculate the ratio of Hedls puncta count in KapB-expressing cells to the vector control for each treatment condition. (F) Representative images of cells stained for PB-resident protein Hedls (green), KapB (blue), and F-actin (red, phalloidin). Boxes indicate area shown in the Hedls (zoom) panel. Scale bar represents 20 μm. Statistics were determined using ratio paired t-tests between control and experimental groups; error bars represent standard deviation; n=3 independent biological replicates; * = $p < 0.05$, ** = $p < 0.01$, *** = $p < 0.001$.

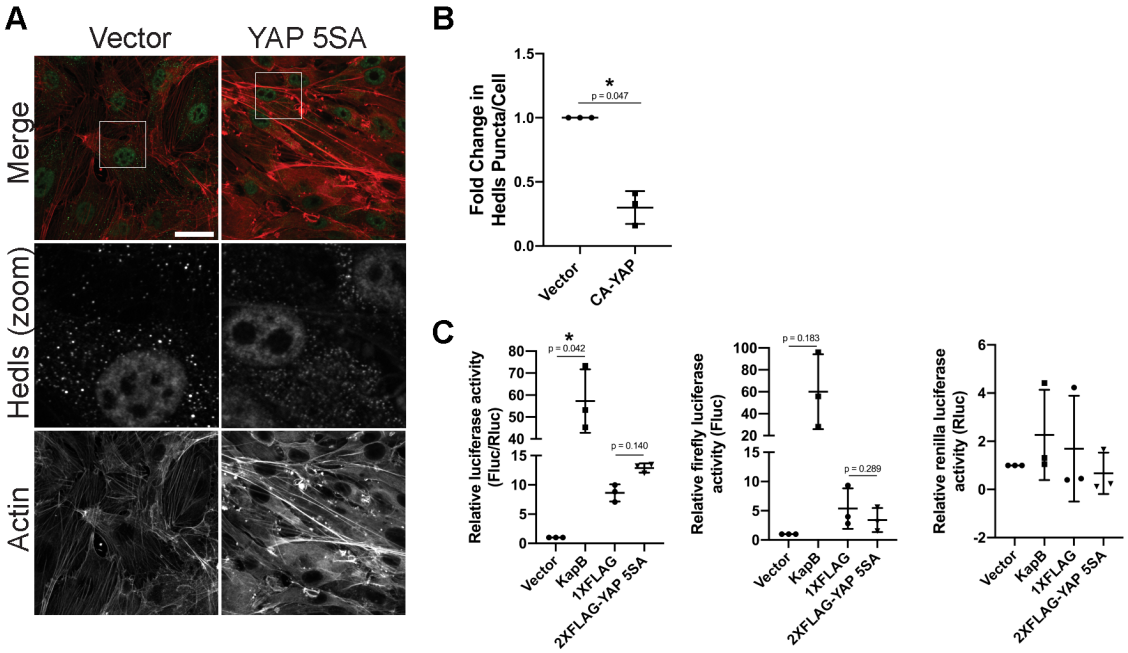

Figure 5: Active YAP elicits PB disassembly. (A, B) HUVECs were transduced with YAP 5SA-expressing and empty vector lentivirus and selected. Cells were fixed for immunofluorescence. (A) Representative images of cells stained for PB-resident protein Hedls (green) and F-actin (red, phalloidin). Boxes indicate area shown in the Hedls (zoom) panel. Scale bar represents 20 μm. (B) Fixed cells were stained for CellProfiler analysis as detailed in the methods. The number of Hedls puncta per cell was quantified and normalized to the vector control. (C) HeLa Tet-Off cells were seeded and co-transfected with an ARE-containing Firefly luciferase (Fluc) reporter plasmid, a Renilla luciferase (Rluc) reporter plasmid lacking an ARE, and either a KapB, YAP 5SA expression plasmid or vector controls. At 36 h post-transfection, transcription was terminated with doxycycline treatment for 12 h. Fluc and Rluc activity was measured. Data is normalized to vector control within each replicate. Graphs show the ratio of Fluc to Rluc, independent Fluc values and independent Rluc values, respectively. Statistics were determined using ratio paired t-tests between control and experimental groups (B) or repeated measures ANOVA (C); error bars represent standard deviation; n=3 independent biological replicates; * = $p < 0.05$, ** = $p < 0.01$.

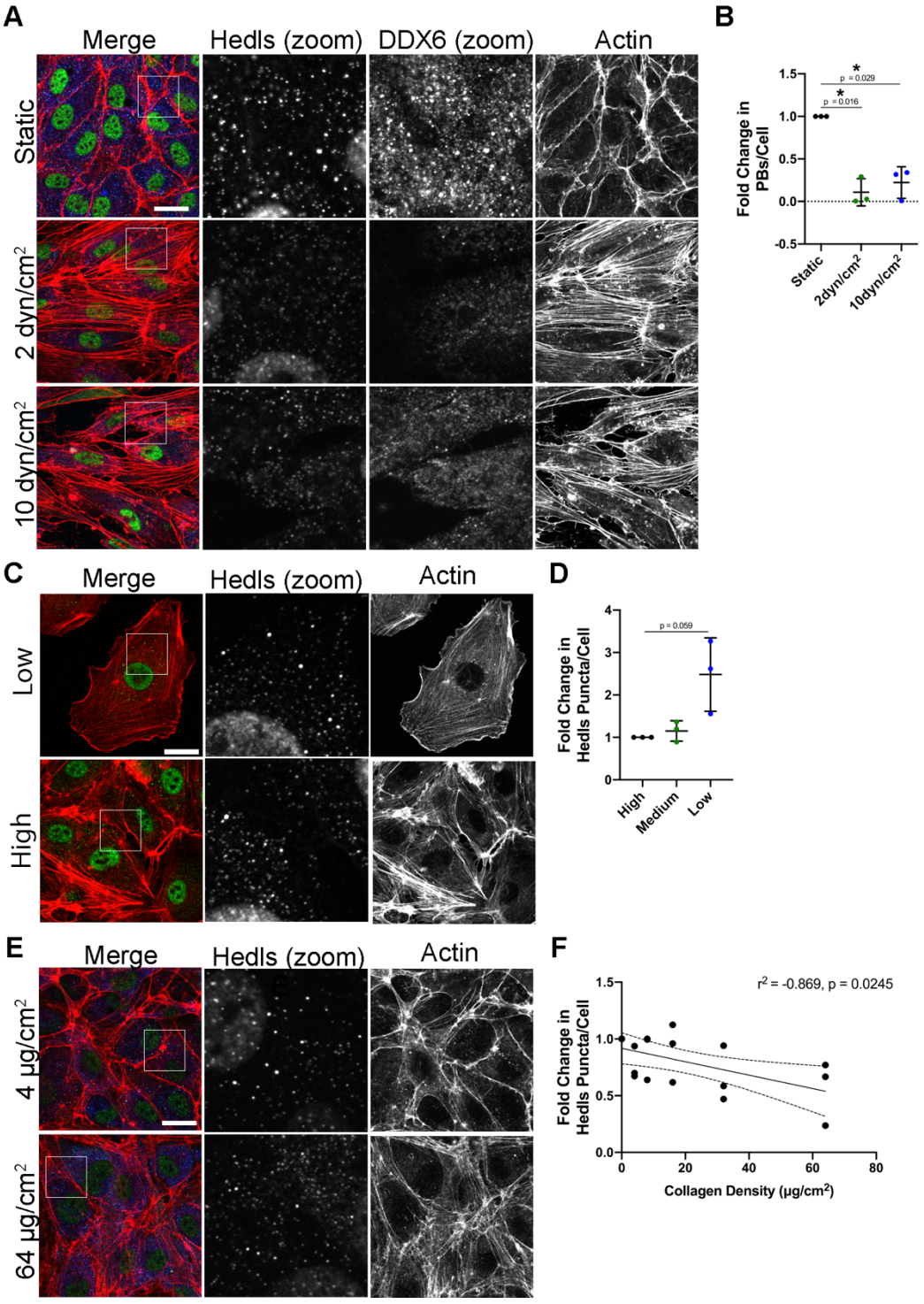

Figure 6: YAP Inputs Mediate PB Disassembly. (A, B) HUVECs were seeded onto collagen-coated microscope slides and exposed to shear stress of 2 dyn/cm^2, 10 dyn/cm^2 or no shear (static control) for 21 h. Cells were fixed and stained for immunofluorescence. (A) Representative images of cells stained for PB-resident proteins Hedls (green) and DDX6 (blue), as well as F-actin (red, phalloidin). Boxes indicate area shown in Hedls (zoom) and DDX6 (zoom) panels. Scale bar represents 20 μm. (B) CellProfiler was used to count nuclei, Hedls puncta and DDX6

puncta. In RStudio analysis, puncta with ≥ 70% correlation between Hedls and DDX6 (PBs) were counted and normalized to number of nuclei per condition. PB counts were normalized to static control within each replicate. (C, D) HUVECs were split and seeded at a high-, medium- and low-density, cultured for 48 h and fixed for immunofluorescence. (C) Representative images of cells stained for the PB-resident protein Hedls (green) and F-actin (red, phalloidin). Boxes indicate images shown in Hedls (zoom) panel. Scale bar represents 20 μm. (D) Fixed cells were stained for CellProfiler analysis as detailed in the methods. The number of Hedls puncta per cell was quantified and normalized to the high confluence condition. (E, F) Coverslips were coated for 4 h with 0 to 64 μg/cm^2 of collagen. HUVECs were grown for 72 h on coated coverslips and fixed for immunofluorescence. (E) Representative images of cells stained for PB-resident protein Hedls (green), DDX6 (blue) and F-actin (red, phalloidin). Boxes indicate images shown in Hedls (zoom) panel. Scale bar represents 20 μm. (F) Fixed cells were stained for CellProfiler analysis as detailed in the methods. The number of Hedls puncta per cell was quantified and normalized to the 0 μg/mL collagen-coating condition. Statistics were determined using repeated measures ANOVA (A, B) or Pearson's correlation co-efficient (C); error bars represent standard deviation (A, B) and 95% confidence interval of line of best fit (slope is significantly non-zero, $p = 0.014$) (C); n=3 independent biological replicates; * = $p < 0.05$, ** = $p < 0.01$.

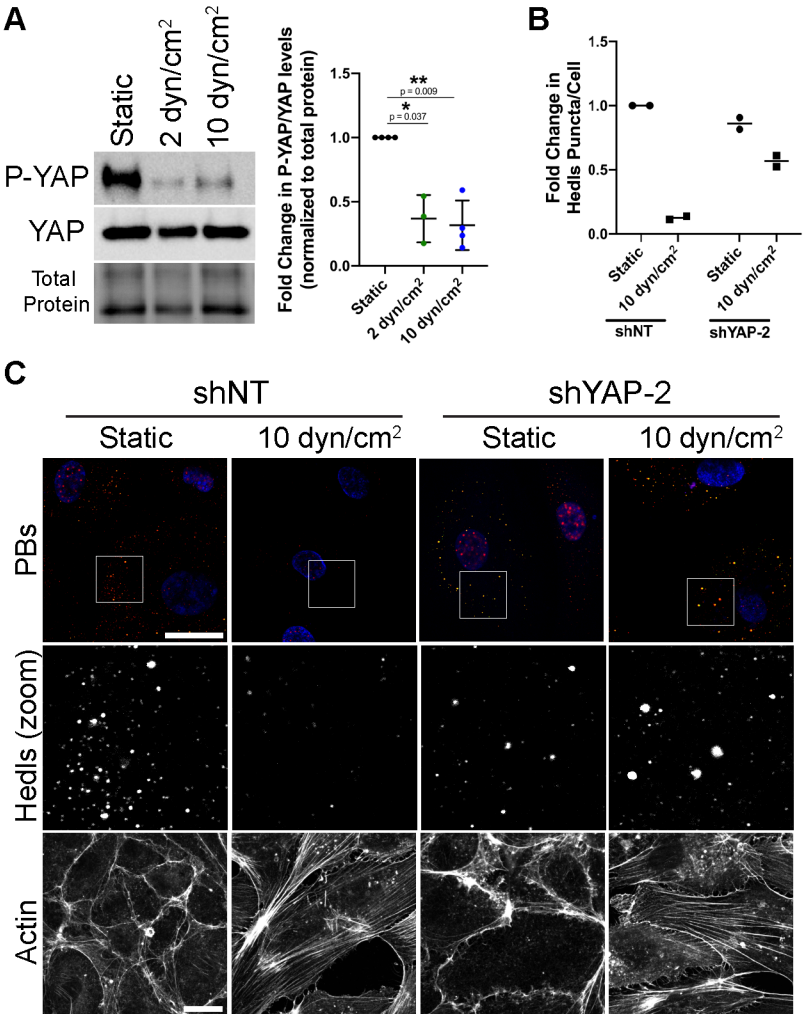

Figure 7: YAP is required for Hedls puncta disassembly in HUVECs subjected to shear stress. (A) HUVECs were seeded onto collagen-coated microscope slides and exposed to shear stress of 2 dyn/cm^2, 10 dyn/cm^2 or a static control for 21 h. Cells were lysed for immunoblotting. One representative immunoblot and quantification of three independent experiments stained with P(S127)-YAP- and YAP-specific antibody is shown. P(S127)-YAP and YAP protein levels in each condition were normalized to total protein. All treatments were normalized to static control within each replicate. (B, C) HUVECs were transduced with shRNAs targeting YAP (shYAP-2) or with a non-targeting (shNT) control and selected. Cells were seeded onto collagen-coated microscope slides and exposed to shear stress of 10 dyn/cm^2 or no shear (static control) for 21 h. Cells were fixed and stained for immunofluorescence. (B) CellProfiler was used to count nuclei and Hedls puncta. In RStudio analysis, Hedls puncta were normalized to number of nuclei per condition. Hedls puncta counts were normalized to static control. (C) Representative images of cells stained for PB-resident protein Hedls (red), DDX6 (green) and DAPI (blue). In parallel, separate coverslips were stained for F-actin (phalloidin). Boxes indicate area shown in the Hedls (zoom) panel. Scale bar represents 20 μm. Statistics were determined using repeated measures ANOVA (A); error bars represent standard deviation (A) ; n=4, except 2 dyn/cm^2 (n=3) (A) and n = 2 (B, C) independent biological replicates; * = $p < 0.05$, ** = $p < 0.01$.

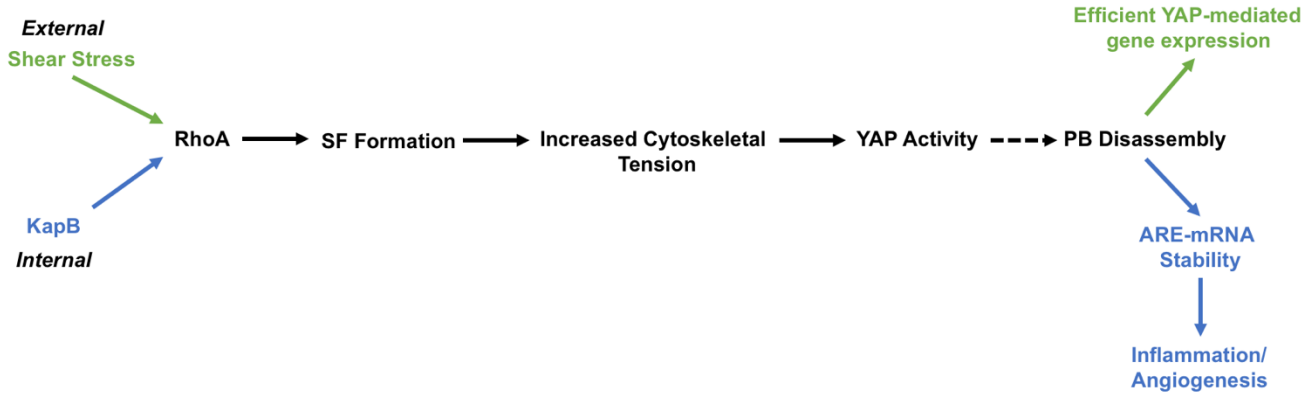

Figure 8: KapB activates a mechanoresponsive pathway from within the cell rather than without to mediate PB disassembly. Cells respond to external mechanical force by activating their structural support network, the actin cytoskeleton. The GTPase RhoA and its downstream effectors coordinate this response, bundling actin filaments into stress fibers (SFs), enhancing actomyosin contractility and increasing adhesion to the underlying matrix to help withstand force-induced membrane deformation. Together, these actin-based responses increase cytoskeletal tension and elicit the dephosphorylation and nuclear translocation of the mechanoresponsive transcription activator YAP where it collaborates with other transcription factors to induce TEAD-responsive genes. We present data to support the existence of a novel mechanoresponsive pathway that links actin SFs, actomyosin contractility, and the transcription transactivator YAP to the disassembly of PBs. The viral protein KapB taps into this mechanoresponsive pathway to trigger mechanical changes to cytoskeletal structures and downstream effectors that would normally respond to force, thereby inducing PB disassembly from within the cell, rather than from without.

Supplementary Information

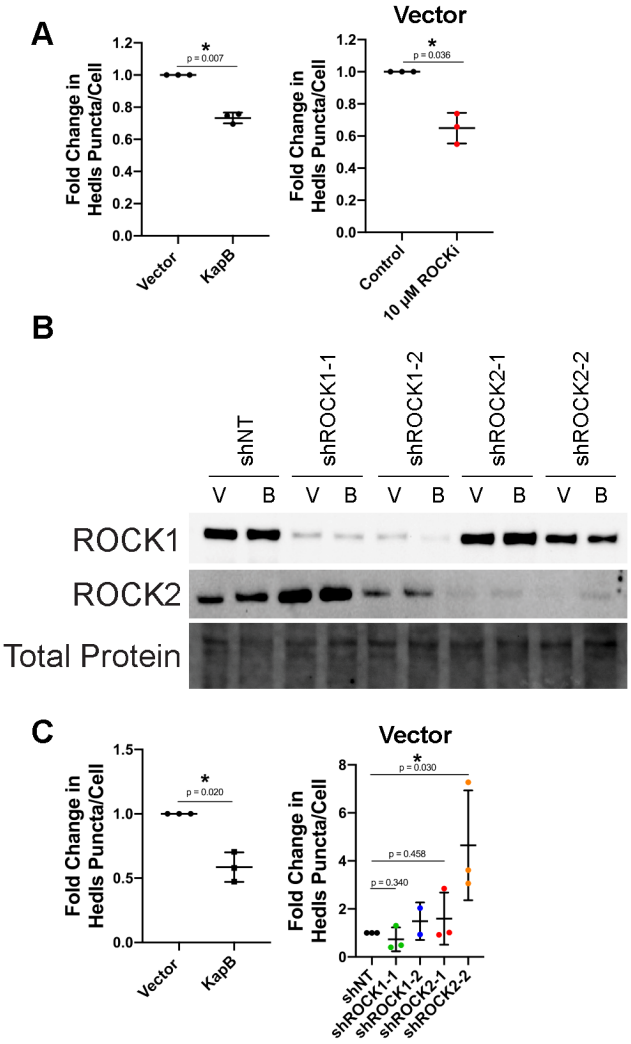

Figure S1: The RhoA-effector ROCK is required for KapB-mediated PB disassembly, knockdown confirmation and vector data. (A) KapB- and vector- expressing HUVECs were treated with 10 μM Y-27632 or water control for 4 h and fixed for immunofluorescence. Fixed cells were stained for CellProfiler analysis as detailed in the methods. The number of Hedls puncta per cell was quantified and normalized to the vector control. Vector control data is shown. (B, C) KapB- and vector- expressing HUVECs were transduced with shRNAs targeting ROCK1 and ROCK2 (shROCK1-1, shROCK1-2, shROCK2-1, shROCK2-2) or with a non-targeting (shNT) control and selected. In parallel, cells were lysed for immunoblotting or fixed for immunofluorescence. (B) One representative immunoblot of three independent experiments stained using ROCK1- and 2-specific antibodies. (C) Fixed cells were stained for CellProfiler analysis as detailed in the methods. The number of Hedls puncta per cell was quantified and normalized to the vector NT control within each replicate. Vector control data is shown. Statistics were determined using a ratio paired t-test between control and experimental groups; error bars represent standard deviation; n=3 independent biological replicates; * = $p < 0.05$.

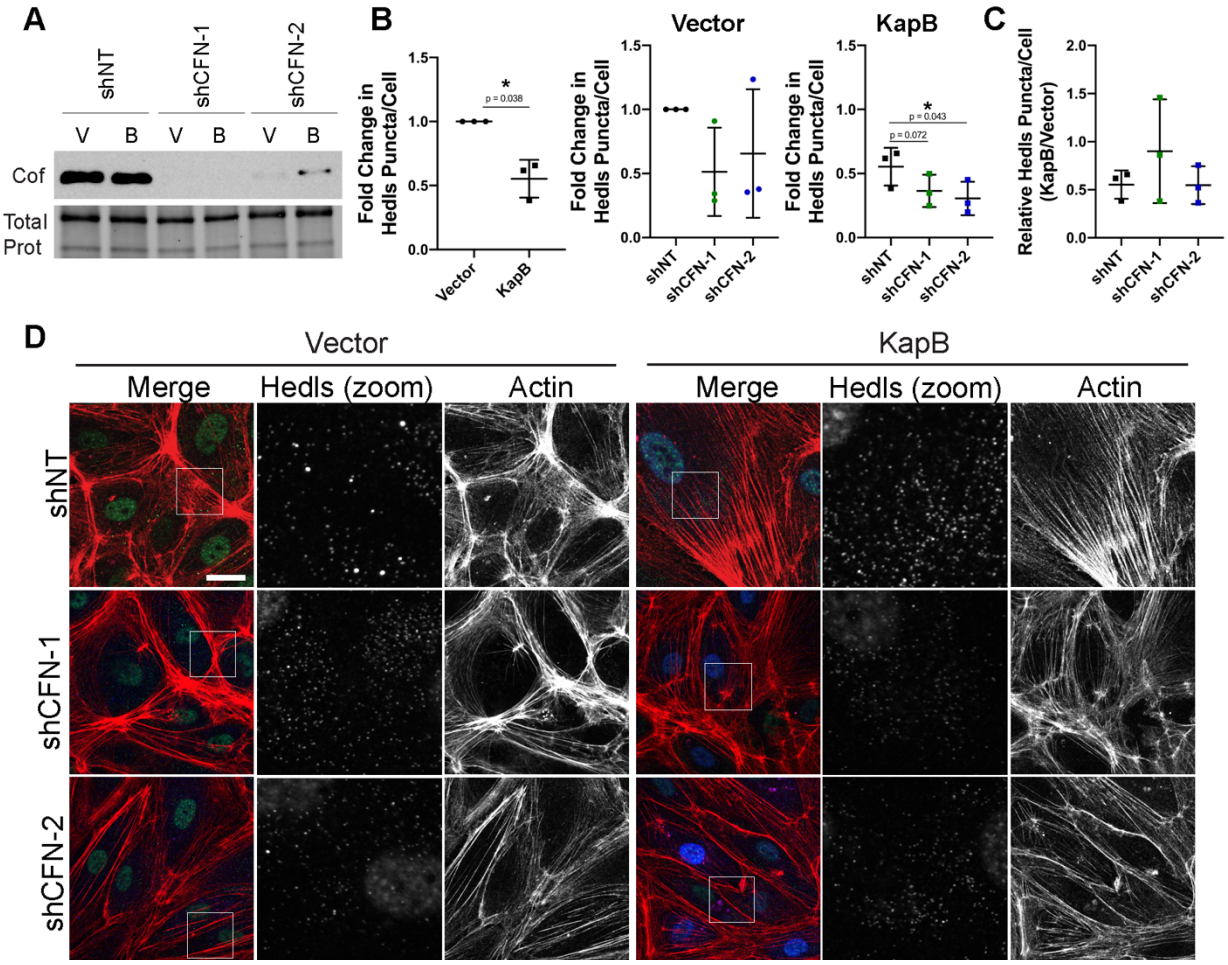

Figure S2: Cofilin knockdown augments KapB-mediated PB disassembly. KapB- and vector- expressing HUVECs were transduced with shRNAs targeting cofilin (shCFN-1, shCFN-2) or with a non-targeting (shNT) control and selected. In parallel, cells were fixed for immunofluorescence or lysed for immunoblotting. (A) One representative immunoblot of three independent experiments stained using a cofilin-specific antibody. (B, C) Fixed cells were stained for CellProfiler analysis as detailed in the methods. (B) The number of Hedls puncta per cell was quantified and normalized to the vector NT control within each replicate. (C) CellProfiler data was used to calculate the ratio of Hedls puncta counts in KapB-expressing cells versus the vector control for each treatment condition. (D) Representative images of cells stained for PB-resident protein Hedls (green), KapB (blue), and F-actin (red, phalloidin). Boxes indicate the area of the field of view that is shown in Hedls (zoom) panel. Scale bar represents 20 μm. Statistics were determined using a ratio paired t-test between control and experimental groups; error bars represent standard deviation; n=3 independent biological replicates; * = $p < 0.05$.

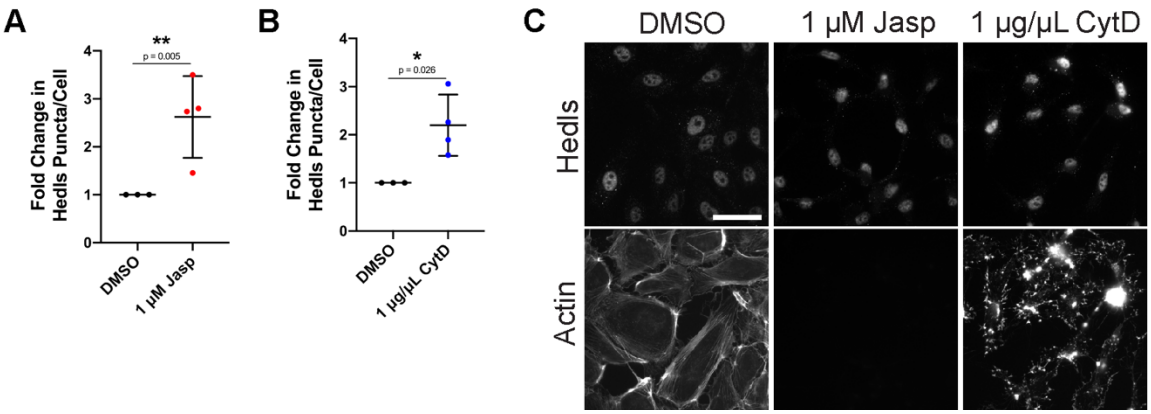

Figure S3: G-actin concentration does not control PB disassembly. (A, B, C) HUVECs were treated with 1 μM Jasp (polymerizes actin and decreases monomeric G-actin), 1 μg/μL CytD (actin depolymerization to increase monomeric G-actin) or a DMSO control for 30 min. (A, B) Fixed cells were stained for CellProfiler analysis as detailed in the methods. The number of Hedls puncta per cell was quantified and normalized to the DMSO control. (C) Representative images of cells stained for PB-resident protein Hedls and F-actin (phalloidin). Actin is not seen in Jasp panel due to Jasp-mediated interference with phalloidin staining (Bubb et al. 1999). Scale bar represents 20 μm. Statistics were determined using a ratio paired t-test between control and experimental groups; error bars represent standard deviation; n=3 independent biological replicates; * = $p < 0.05$, ** = $p < 0.01$.

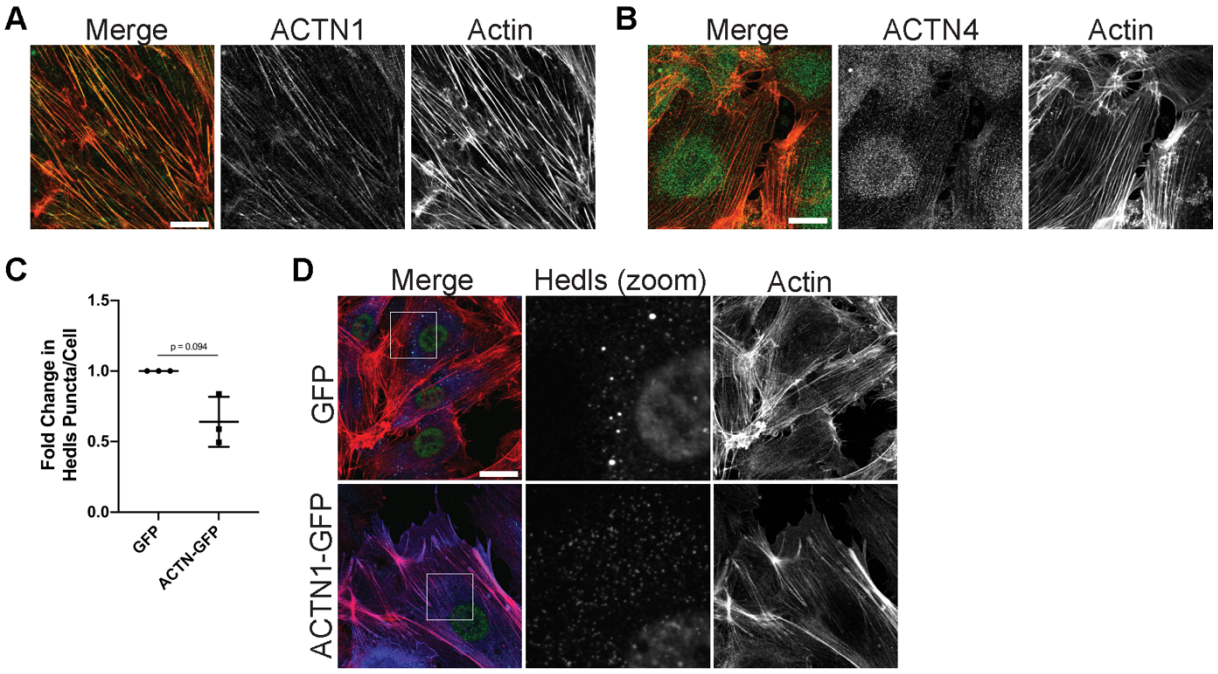

Figure S4: α-actinin-1-overexpression mediated SF formation and PB disassembly. HUVECs were fixed and stained with antibodies for (A) α-actinin-1 and (B) α-actinin-4. (C, D) HUVECs transduced with recombinant lentiviruses expressing GFP-tagged α-actinin-1 (ACTN-GFP) or a GFP control were selected and fixed for immunofluorescence. (C) Fixed cells were stained for CellProfiler analysis as detailed in the methods. The number of Hedls puncta per cell was quantified and normalized to the vector GFP control. (D) Representative images of cells stained for PB-resident protein Hedls (false-coloured green), ACTN-GFP (false-coloured blue), and F-actin (red, phalloidin). Boxes indicate images shown in Hedls (zoom) panel. Scale bar represents 20 μm. Statistics were determined using a ratio paired t-test between control and experimental groups; error bars represent standard deviation; n=3 independent biological replicates; * = $p < 0.05$.

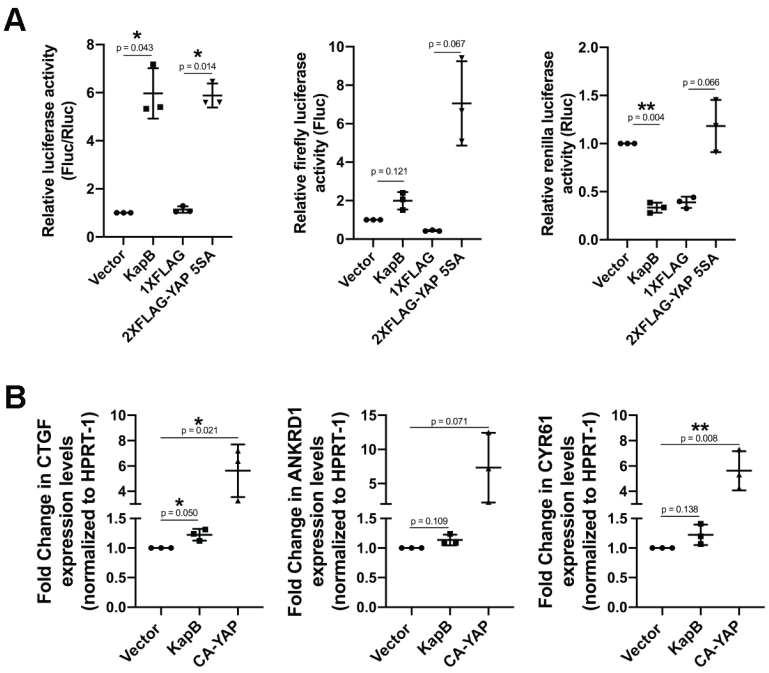

Figure S5: KapB does not induce transcription of canonical YAP-responsive genes. (A) HEK-293A cells were co-transfected with a firefly luciferase (Fluc) reporter plasmid with a YAP-responsive TEAD promoter element, a TREX-renilla luciferase (Rluc) reporter plasmid, and overexpression constructs for either a KapB, YAP 5SA or vector control. At 36 h post-transfection, cells were starved in serum-free DMEM for 12 h, lysed and Fluc and Rluc activity was recorded. Data is normalized to vector control. Graphs show the ratio of Fluc to Rluc, independent Fluc values and independent Rluc values, respectively. (B) HUVECs were transduced with recombinant lentiviruses expressing KapB, a constitutively-active version of YAP (YAP 5SA) or an empty vector control, selected and lysed for total RNA. qRT-PCR analysis of steady state mRNA levels of canonical YAP-regulated genes CTGF, ANKRD1 and CYR61 was performed, and was normalized to steady state HPRT-1 mRNA levels. Statistics were determined using repeated measures ANOVA; error bars represent standard deviation; n=3 independent biological replicates; * = $p < 0.05$, ** = $p < 0.01$.

1419 **Table S1: Antibodies used in this study.**

Antibody	Source	Use	Dilution
Rabbit ⟨-mDia1	Cell Signalling Technologies (Cat#:5486)	Immunoblotting	1:1000 in 2.5% BSA
Rabbit ⟨-ROCK1	Cell Signalling Technologies (Cat#:4035)	Immunoblotting	1:1000 in 2.5% BSA
Rabbit ⟨-ROCK2	Cell Signalling Technologies (Cat#:9029)	Immunoblotting	1:500 in 2.5% BSA
Rabbit ⟨-Cofilin	Cell Signalling Technologies (Cat#:5175)	Immunoblotting	1:1000 in 2.5% BSA
Rabbit ⟨-P-YAP	Cell Signalling Technologies (Cat#: 4911)	Immunoblotting	1:1000 in 2.5% BSA
Rabbit ⟨-YAP	Cell Signalling Technologies (Cat#: 4912)	Immunoblotting	1:1000 in 2.5% BSA
⟨-Mouse IgG, HRP-linked (2˚)	Cell Signalling Technologies (Cat#: 7076)	Immunoblotting	1:2000 to 1:4000 in 2.5% BSA
⟨-Rabbit IgG, HRP-linked (2˚)	Cell Signalling Technologies (Cat#: 7074)	Immunoblotting	1:2000 to 1:4000 in 2.5% BSA

Mouse ⟨-p70 s6 kinase (detects Hedls)	Santa Cruz (Cat#:sc-8418)	Immunofluorescence	1:1000 in blocking buffer (1% Human AB in PBS), 4˚C overnight
Rabbit ⟨-KapB	Gift from D. Ganem and C. McCormick	Immunofluorescence/ Immunoblotting	1:1000 in blocking buffer (1% Human AB in PBS), 30 min RT
Rabbit ⟨-actinin-1	Abclonal (Cat#:A1160)	Immunofluorescence	1:500 in blocking buffer (1% Human AB in PBS), 4˚C overnight
Mouse ⟨-actinin-4	Santa Cruz (Cat#:sc-390205)	Immunofluorescence	1:500 in blocking buffer (1% Human AB in PBS), 4˚C overnight
Mouse ⟨-YAP	Santa Cruz (Cat#:sc-101199)	Immunofluorescence	1:1000 in blocking buffer (1% Human AB in PBS), 4˚C overnight
Rabbit ⟨-DDX6	Bethyl Labs (Cat#:A300-461A)	Immunofluorescence	1:1000 in blocking buffer (1% Human AB in PBS), 4˚C overnight
Alexa Fluor 555-conjugated donkey ⟨-mouse IgG (2˚)	Invitrogen (Cat#:A31570)	Immunofluorescence	1:1000 in blocking buffer (1% Human AB in PBS), 1h RT
Alexa Fluor 488-conjugated chicken ⟨-rabbit IgG (2˚)	Invitrogen (Cat#:A21441)	Immunofluorescence	1:1000 in blocking buffer (1% Human AB in PBS), 1h RT
Alexa Fluor 555-conjugated donkey ⟨-rabbit IgG (2˚)	Invitrogen (Cat#:A31572)	Immunofluorescence	1:1000 in blocking buffer (1% Human AB in PBS), 1h RT
Alexa Fluor 488-conjugated chicken ⟨-mouse IgG (2˚)	Invitrogen (Cat#:A21200)	Immunofluorescence	1:1000 in blocking buffer (1% Human AB in PBS), 1h RT

1420
1421
1422

1423 **Table S2: Plasmids used in this study.**

Plasmid Name	Use	Source	Bacterial Selection Cassette	Mammalian Selection Cassette (Lentiviral Plasmids Only)
pLJM-1-EV	Control vector for lentiviral expression studies	C. McCormick (Dalhousie University)	Ampicillin	Blasticidin, Puromycin
pLJM-1 KapB	Lentiviral expression of KapB	C. McCormick (Dalhousie University)	Ampicillin	Blasticidin
pLKO-(shRNA)	Lentiviral expression of short hairpin RNAs (shRNA sequences in Table S3)	Cloned from: pLKO-TRC Addgene no.: 26655	Ampicillin	Puromycin
pLJM-1 ⟨-actinin1-GFP	Lentiviral expression of ⟨-actinin1-GFP	Cloned from: pEGFP-N1 ⟨-actinin-1, Addgene no.: 11908	Ampicillin	Puromycin
pLJM-1-YAP-5SA (CA-YAP)	Lentiviral expression of constitutively active YAP	Cloned from: p2XFLAG-YAP-5SA, Donated by C. McCormick (Dalhousie University)	Ampicillin	Blasticidin
pcDNA3.1	Transfection control	Invitrogen	Ampicillin	N/A
pcDNA3.1 KapB	Transfection of KapB	C. McCormick (Dalhousie University)	Ampicillin	N/A

p1XFLAG	Transfection control	Cloned from: p2XFLAG-YAP-5SA, Donated by C. McCormick (Dalhousie University)	Ampicillin	N/A
p2XFLAG-YAP 5SA	Transfection of YAP 5SA	Donated by C. McCormick (Dalhousie University)	Ampicillin	N/A
pMD2.G	Envelope protein for lentiviral production	Addgene no.: 12259	Ampicillin	N/A
psPAX2	Packaging proteins for lentiviral production	Addgene no.: 12260	Ampicillin	N/A

1428 **Table S3: shRNA sequences used in this study.**

Target	Sequence (5' – 3')
Non-targeting sense	CCGGAGCACAAGCTGGAGTACAACTACTCGAGATCAACATGAGGTCGAACACGATTTG
Non-targeting antisense	AATTCAAAAAGCACAAGCTGGAGTACAACTAATCAACATGAGGTCGAACACGATTTG
mDia1 sh1 sense	CCGGCCAATTCTGCTCATAGAAATTCTCGAGAATTTCTATGAGCAGAATTGGTTTTTG
mDia1 sh1 antisense	AATTCAAAAACCAATTCTGCTCATAGAAATTCTCGAGAATTTCTATGAGCAGAATTGG
mDia1 sh2 sense	CCGGAAGATGACGTTGTTACACTTCCTCGAGGAAGTGTAACAACGTCATCTTTTTTTG
mDia1 sh2 antisense	AATTCAAAAAAAGATGACGTTGTTACACTTCCTCGAGGAAGTGTAACAACGTCATCTT
ROCK1 sh1 sense	CCGGAAGATGACGTTGTTACACTTCCTCGAGGAAGTGTAACAACGTCATCTTTTTTTG
ROCK1 sh1 antisense	AATTCAAAAAAAGATGACGTTGTTACACTTCCTCGAGGAAGTGTAACAACGTCATCTT
ROCK1 sh2 sense	CCGGAAGATGACGTTGTTACACTTCCTCGAGGAAGTGTAACAACGTCATCTTTTTTTG
ROCK1 sh2 antisense	AATTCAAAAAAAGATGACGTTGTTACACTTCCTCGAGGAAGTGTAACAACGTCATCTT
ROCK2 sh1 sense	CCGGCGTTGCCATATTAAGTGTCATCTCGAGATGACACTTAATATGGCAACGTTTTTG
ROCK2 sh1 antisense	AATTCAAAAACGTTGCCATATTAAGTGTCATCTCGAGATGACACTTAATATGGCAACG
ROCK2 sh2 sense	CCGGGCCTTGCATATTGGTCTGGATCTCGAGATCCAGACCAATATGCAAGGCTTTTTG
ROCK2 sh2 antisense	AATTCAAAAAGCCTTGCATATTGGTCTGGATCTCGAGATCCAGACCAATATGCAAGGC

Cofilin sh1 sense	CCGGACGACATGAAGGTGCGTAAGTCTCGAGACTTACGCACCTTCATGTCGTTTTTTG
Cofilin sh1 antisense	AATTCAAAAAACGACATGAAGGTGCGTAAGTCTCGAGACTTACGCACCTTCATGTCGT
Cofilin sh2 sense	CCGGCCAGATAAGGACTGCCGCTATCTCGAGATAGCGGCAGTCCTTATCTGGTTTTTG
Cofilin sh2 antisense	AATTCAAAAACCAGATAAGGACTGCCGCTATCTCGAGATAGCGGCAGTCCTTATCTGG
YAP sh1 sense	CCGGCTGGTCAGAGATACTTCTTAACTCGAGTTAAGAAGTATCTCTGACCAGTTTTTC
YAP sh1 antisense	AATTGAAAAACTGGTCAGAGATACTTCTTAACTCGAGTTAAGAAGTATCTCTGACCAG
YAP sh2 sense	CCGGAAGCTTTGAGTTCTGACATCCCTCGAGGGATGTCAGAACTCAAAGCTTTTTTTC
YAP sh2 antisense	AATTGAAAAAAAGCTTTGAGTTCTGACATCCCTCGAGGGATGTCAGAACTCAAAGCTT

1429
1430
1431

1432 **Table S4: Drug treatments used in this study.**

Drug	Use	Source (Cat#)	Concentration Used	Duration
Y-27623 dihydrochloride (ROCKi)	Non-isoform specific inhibition of ROCK	Sigma-Aldrich (Cat#:Y0503)	10 μM	4 h
Jasplakinolide	Aberrant polymerization of actin, decreasing monomeric G-actin	Sigma-Aldrich (Cat#:J4580)	0.5 μM, 1 μM	30 min
Cytochalasin D	Inhibition of actin polymerization, increasing monomeric G-actin	Sigma-Aldrich (C8273)	1 μg/mL	30 min
(-)-Blebbistatin	Inhibition of MLC contractility	Sigma-Aldrich (Cat#:B0560)	10 μM	30 min
Calyculin A	Inhibition of MLC phosphatase, resulting in cell contraction	Abcam (Cat#: ab141784)	2.5 nM, 5 nM	20 min

1433

1434

1435 **Table S5: qRT-PCR primers used in this study.**

Target	Forward/ Reverse	Sequence	Tm (˚C)	Reference
CYR61	Forward	ATGGTCCCAGTGCTCAAAGA	60	(K.-C. Wang et al. 2016)
CYR61	Reverse	GGGCCGGTATTTCTTCACAC	62	(K.-C. Wang et al. 2016)
CTGF	Forward	CAGCATGGACGTTCGTCTG	60	(K.-C. Wang et al. 2016)
CTGF	Reverse	AACCACGGTTTGGTCCTTGG	62	(K.-C. Wang et al. 2016)
CTGF	Forward	CCCTCGCGGCTTACCG	56	(K.-C. Wang et al. 2016)
CTGF	Reverse	GGACCAGGCAGTTGGCTCT	62	(K.-C. Wang et al. 2016)
ANKRD1	Forward	ACGCCAAAGACAGAGAAGGA	60	(K.-C. Wang et al. 2016)
ANKRD1	Reverse	TTCTGCCAGTGTAGCACCAG	52	(K.-C. Wang et al. 2016)
HPRT-1	Forward	CTTTCCTTGGTCAGGCAGTATAA	66	(Singh, 2019)
HPRT-1	Reverse	AGTCTGGCTTATATCCAACACTTC	60	(Singh, 2019)
HPRT-1	Forward	TGGCGTCGTGATTAGTGATG	64	(Singh, 2019)
HPRT-1	Reverse	GACGTTCAGTCCTGTCCATAAT	68	(Singh, 2019)

1436